AUT Journal of Modeling and Simulation

AUT J. Model. Simul., 55(1) (2023) 71-98
DOI: 10.22060/miscj.2023.21867.5305

Linear/Nonlinear PID Control of Cooperative Multiple Robot Manipulators: A Robust Approach

A. Izadbakhsh[1]*, N. Nasiri[2], M. B. Menhaj[3]

[1] Department of Electrical Engineering, Garmsar Branch, Islamic Azad University, Garmsar, Iran.

[2] Department of Electrical Engineering, Qazvin Branch, Islamic Azad University, Qazvin, Iran.

[3] The Center of Excellence on Control and Robotics, Department of Electrical Engineering, Amirkabir University of Technology (Tehran Polytechnic), Tehran, Iran.

ABSTRACT: The issue of position/force control of collaborative robotic systems moving a payload is proposed in this paper. The proposed approach must be able to maintain the orientation/position of the payload on the reference trajectory while applying a limited force to the object through the robot's end-effector. With this in mind, linear/nonlinear PID control schemes have been proposed to achieve accurate and robust tracking performance. Lyapunov's stability analysis is utilized to confirm the stability of the controlled system. It proves that the controlled system is stable, while the object's orientation/position tracking errors are uniformly ultimately bounded (UUB) in any bounded region of state space. It also presents some conditions for proper selection of the linear/nonlinear PID controllers' gains in the form of two theorems. The proposed controllers apply to two coordinated 3DOF robotic arms that carry a payload. The simulation results tested two types of trajectories, including simple and complex paths. The results are also compared to those of a strong state-of-the-art approximator, the Chebyshev Neural Network (CNN).

Review History:

Received: Oct. 20, 2022
Revised: May, 07, 2023
Accepted: May, 18, 2023
Available Online: Oct. 10, 2023

Keywords:

Robust position control
PID Controller
Nonlinear PID Controller
Cooperative manipulators

1- Introduction

Human life has been profoundly impacted by the development of robotic systems on both social and economic levels. These systems are used in service centers, medical clinics, and factory production lines because of their great speed and precise operation. Many of these activities cannot be completed by one robot and need a team of arms, mobile robots, and unmanned aerial vehicles (UAVs) [1-5]. Packing, assembling, painting, welding, and, handling, for example, all necessitate the employment of several robot arms with great precision and dexterity. Because of their significance, a variety of model-based control mechanisms have emerged for these robots [6-7].

Model-based control schemes are designed based on precise system modeling. It is noteworthy that the dynamic equations describing the behavior of collaborative robotic systems are very complex and pose many challenges in their use of them. This complexity is related to Inertia matrices, the Coriolis and centrifugal matrices, and finally, the gravity vectors that include the robot Jacobin matrices, inverse, and their derivatives. This problem becomes hypersensitive, especially to increasing degrees of freedom of collaborative robotic systems. The existence of all these problems, along with the unavailability of accurate parametric information of the robotic system due to changes in load conditions, external disturbances, and measuring equipment, limits and renders model-based techniques inefficient. This fact has led researchers toward using neuro-fuzzy controllers [8].

To operate cooperative robotic arms, Hu et al. used neural networks and a Markovian switching network to create an adaptive controller [9]. It is assumed that the controlled system is exponentially stable. A zeroing neural network is employed in [10] to fulfill a cooperative path tracking of mobile manipulators. Using an intelligent optimization method, the controller is then optimized. To tackle the cooperative arms tracking problem, Wu et al. suggested a predictive controller using neural networks [11]. The uncertainty is treated as a perturbation in this work, and an extended observer is utilized to limit their impact. [12] proposes a fuzzy sliding mode approach as a solution to the problem of cooperating arms moving an item. In this study, the cooperating system dynamics are decomposed using the passive decomposition approach. Li et al., establish an admission model for cooperating robotic manipulators that carry an item [13]. Following that, to estimate the uncertainty, an adaptive neural network is employed. The system stability is also assured. The fuzzy adaptive control described in [14] is meant to complete a task that requires the collaboration of nonlinear planar robots without the risk of collision. The controller-approximator structure is proposed so that it compensates for the lumped uncertainties and fulfills the cooperative task efficiently. The goal of [15] is to provide

*Corresponding author's email: izadbakhsh_alireza@hotmail.com

a distributed control approach for networked arms to collaboratively move an un-modelled object without the need for force measurements. In this study, an adaptive control technique is developed using the wavelet neural network to estimate unknown dynamics of the system, while keeping the controlled system stable. In [16], a decentralized control approach for a large object movement using a team of robots is proposed. A deep Q-network controller is designed to equip each robot. A function approximator is developed for the system based on neural networks, which takes continuous states into account and provides a robust system performance.

While fuzzy systems and neural networks may estimate multiple functions based on their universal approximation characteristic, they suffer limitations that turn their design and construction into a difficult problem [17-18]. In fuzzy logic-based approximators, various parameters such as types and numerical ranges of membership functions, methods of fuzzification/defuzzification, the inference system, and the rule database, should be chosen properly to fulfill the design objectives. In neural network-based approximators, factors such as the network structure, number of hidden layers/neurons, and activation function type should be selected properly. All of these factors need significant design expertise, and their complicated structure causes difficulty in applying them, increasing the system's computational load.

Considering literature on the field of robust control dealing with uncertainty has a great deal of importance. Hence, several studies have been dedicated to this field of research [19-25]. Nasiri et al. proposed an observer-based robust suboptimal controller in a State-Dependent Riccati Equation (SDRE) framework to deal with parametric uncertainty and external disturbances for robot manipulators [19]. In [20], a combination of SDRE with Fourier series is presented to deal with lumped uncertainties and disturbances [20]. A robust optimal scheme is applied to Electrical Flexible-Joint Robots (EFJRs) based on utilizing SDRE in designing the sliding surface of SMC [21]. To handle uncertainty and disturbances an uncertain psudeo-linear structure is proposed for robust optimal schemes and applied to cooperative manipulators [22]. A robust H-infinity controller is proposed in [23] for cooperative manipulators. A novel PID controller is introduced in [24] to solve (globally) the position and orientation consensus-based formation problem of multiple nonholonomic vehicles modeled as differential drive robots affected by external disturbances. PID and Fractional Order PID (FOPID) controllers are used to obtain a robust controller for the system of the Pioneer-3 Mobile Robot as a complex non-linear system [25].

As a simple controller that is easy to design and implement, PID controllers are very favorite and widely used in the industry. However, high-performance control under changes in environmental parameters and operating conditions is beyond the capabilities of these controllers. Therefore, many scientists are trying to modify the robustness of these controllers [31-32]. Nonlinear PID controllers can be seen as an attempt to modify the efficiency of conventional PID controllers. Reference [33] proposed a FeedForward nonlinear PID control strategy for the performance improvement of the flexure-based micromanipulator systems using a Preisach hysteresis compensator. The mentioned control strategy has been composed of three components: a nonlinearity tracking differentiator, an extended state observer, and finally a nonlinear state error feedback. A nonlinear PID control strategy has been proposed to improve the control performance of a manipulator actuated by a pneumatic muscle actuator [34]. However, no stability analysis has been provided in either of the above-mentioned control strategies. Fuzzy systems and neural networks have been utilized to adjust the gains of nonlinear PID controllers [35]. However, they increase the computational load of the controller whereas they have many parameters that should be tuned. In addition to this, there exist some other problems as mentioned in [17].

Reviewing the literature on previously published papers on neural networks, fuzzy, and PID controllers there is no doubt that simple PID design for the complicated cooperative manipulators dynamics is a great challenge to be dealt with. Some of the PID strategies can be mentioned as PID for n-link rigid robot manipulators under payload variations [36], nonlinear PID based on hypersensitivity criteria for aircraft control [37], adaptive PID with gains tuned based on deep deterministic policy for rigid robot [38], using reinforcement learning in conjunction with PID to position/force control of rigid manipulators [39] and so on.

The current study presents linear/nonlinear robust PID control schemes for cooperating robots. There are two approaches to cope with the complexity introduced by the dynamics of cooperative robot manipulators [40]:

1) Computing control gains independently for each robotic arm.

2) Obtaining control gains for the entire system.

As mentioned in [40], the second case is more complicated and is recommended for at most four cooperative arms. However, the first case is superior for more than four arms because of its experimental implementation capability. The reason for superiority in experimental implementation is that failure of one controller does not ruin the performance of all systems to preserve more safety for the system. As mentioned in [40] in ordinary situations, both methods provide the same output but with different computation times. In singularity points, the first case only quits the singular-situated manipulator, though the second case in the same event shuts down the entire work [40]. However, in this paper, this situation is predicted and handled by considering simultaneously working all the manipulators connected to a payload. The benefits of the proposed linear/nonlinear robust PID techniques over neuro-fuzzy and dynamic model-based methodologies make them appropriate candidates for confronting disturbances and uncertainty. The most important benefits are: (1) Variations in model-based controller parameters may have a considerable effect on system efficiency. In contrast, proposed control approaches do not rely on the system's model except for the upper and lower bound of the system parameters. (2) Projection techniques are

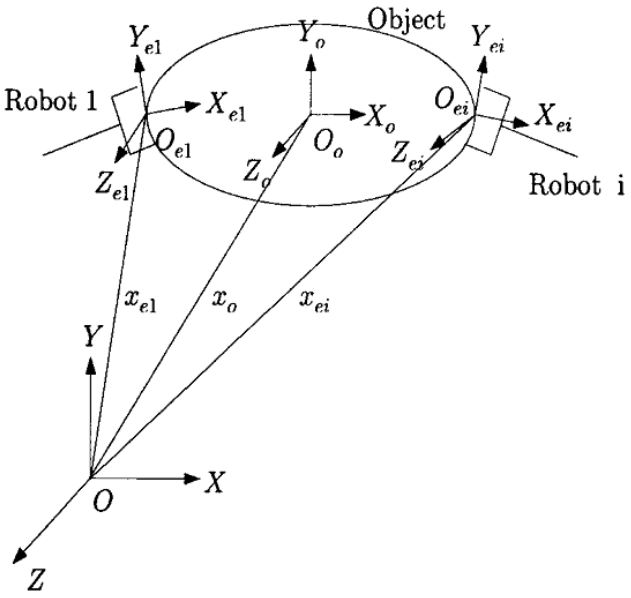

Fig. 1. Different coordinate frames of the system

employed in neuro-fuzzy techniques to keep the parameter values within a specified bound, which increases the system's computational load. The proposed approach is innocent of this issue. (3) Unlike recently mentioned methods, which often require the use of a compensator term including a lot of adjustable parameters in their structure, there exist few control parameters in the proposed linear/nonlinear PID controllers. Consequently, the complexity of the proposed approach is significantly less than other fuzzy or neural network-based approaches.

Based on these discussed advantages, the aim of this paper is linear/nonlinear PID controller design for cooperative manipulators. The stability evaluation is made utilizing the Lyapunov lemma to validate the signals' boundedness. It proves that the controlled system is stable, while the object's orientation/position tracking errors are Uniformly Ultimately Bounded (UUB) in any bounded region of state space. It also retains a constructive algorithm for the proper selection of the linear/nonlinear PID controllers' gains. Finally, the suggested control approaches are used to operate a cooperating robotic system with two arms carrying a rigid load. The simulation results tested two types of trajectories, including simple and complex paths.

The paper sections are arranged as: Section 2 describes the robot dynamic model. It also summarizes the useful properties of the robot dynamics equations. The Linear PID controller design and its stability analysis are presented in Section 3. The proposed nonlinear PID controller structure is discussed in Section 4. Moreover, Section 4 gives a thorough stability evaluation of the controlled system. Section 5 gives the discussions and results, and Section 6 clarifies the significant concluding remarks.

In this paper, $\Re^n$, $\Re^{n\times n}$, and $\Re$ denote the n-dimensional vector space, the $n\times n$ real matrix space, and the real number set, respectively. The norm of matrix $\mathbf{Å}\in\Re^{n\times n}$ and that of vector $\mathbf{z}\in\Re^n$ are defined as $\|\mathbf{Å}\|=\sqrt{\lambda_{\max}(\mathbf{Å}^T\mathbf{Å})}$ and $\|\mathbf{z}\|=\sqrt{\mathbf{z}^T\mathbf{z}}$, respectively. $\lambda_{\max}(\bullet)$ and $\lambda_{\min}(\bullet)$ are the maximum and the minimum eigenvalue of matrix $(\bullet)$. $\mathbf{0}_n$ and $\mathbf{I}_n$ are the $n\times n$ zero and the identity matrices, respectively.

2- Dynamics of Robotic System

2- 1- Preliminaries

Assume m robotic arms with n-degree of freedom (n-DOF) in the workspace are handling a typical item. Fig. 1 shows the various coordinate systems considered for obtaining system dynamics. The OXYZ called base frame is established to indicate the gripper and object locations, as well as their orientations. $\mathrm{O_oX_oY_oZ_o}$ is the object's coordination frame, which is located at the object's mass center. $\mathrm{O_{ei}X_{ei}Y_{ei}Z_{ei}}$ represents the ith robot coordinate frame and is located at its grasp point. The system's dynamic model is supposed to be developed using the following assumptions [26-27].

Assumption 1: The dimensions of the workspace and DOF of each robot are equivalent for all manipulators, indicating that they are non-redundant.

Assumption 2: There is no relative motion between the payload and the robot. i.e. a tight connection between them is considered.

Assumption 3: The manipulator kinematics are known exactly. In addition, the manipulator works to avoid the kinematic singularity. This means that, for each arm, the Jacobian matrix is full-rank and known.

Assumption 4: Due to the rigidity of the payload, exerting forces on the object by grippers does not distort its shape.

2- 2- Robot Model

For the *i*th robot, the dynamics are modeled as follows in the joint space [28]

$$\begin{aligned}&\mathbf{D}_i(\mathbf{q}_i)\ddot{\mathbf{q}}_i+\mathbf{C}_i(\mathbf{q}_i,\dot{\mathbf{q}}_i)\dot{\mathbf{q}}_i\\&+\mathbf{J}_{ei}^T(\mathbf{q}_i)\mathbf{F}_{ei}+\mathbf{G}_i(\mathbf{q}_i)=\boldsymbol{\tau}_i+\boldsymbol{\tau}_{d,i},\end{aligned}\quad \text{i=1,2,...,m} \tag{1}$$

In Equation (1), $\mathbf{q}_i\in\Re^n$ is the generalized coordinate vector of the manipulator. $\mathbf{D}_i(\mathbf{q}_i)\in\Re^{n\times n}$ denotes the positive definite symmetric inertia matrix. $\mathbf{C}_i(\mathbf{q}_i,\dot{\mathbf{q}}_i)\dot{\mathbf{q}}_i\in\Re^{n\times n}$ is the vector of centrifugal and Coriolis forces. $\mathbf{G}_i(\mathbf{q}_i)\in\Re^n$ stands for the vector of gravity forces obtained as the gradient of the robot's potential energy due to gravity. $\tau_i\in\Re^n$ is the vector of controls' torques, $\tau_{d,i}$ represents the external disturbance, $\mathbf{J}_{ei}(\mathbf{q}_i)\in\Re^{n\times n}$ denotes the Jacobian matrix, and finally $\mathbf{F}_{ei}\in\Re^n$ denotes the force applied on the item by the *i*th robot gripper. The concise modeling of the dynamics of the *m* manipulator is represented as follows

$$\mathbf{D}(\mathbf{q})\ddot{\mathbf{q}}+\mathbf{G}(\mathbf{q})+\mathbf{C}(\mathbf{q},\dot{\mathbf{q}})\dot{\mathbf{q}}+\mathbf{J}_e^T(\mathbf{q})\mathbf{F}_e=\boldsymbol{\tau}+\boldsymbol{\tau}_d \tag{2}$$

where

$$\begin{aligned}&\mathbf{q}=\begin{bmatrix}\mathbf{q}_1^T & \dots & \mathbf{q}_m^T\end{bmatrix}^T\in\Re^{mn}\\&\boldsymbol{\tau}=\begin{bmatrix}\boldsymbol{\tau}_1^T & \dots & \boldsymbol{\tau}_m^T\end{bmatrix}^T\in\Re^{mn}\\&\boldsymbol{\tau}_d=\begin{bmatrix}\boldsymbol{\tau}_{d,1}^T & \dots & \boldsymbol{\tau}_{d,m}^T\end{bmatrix}^T\in\Re^{mn}\\&\mathbf{D}(\mathbf{q})=blockdiag\left[\mathbf{D}_1(\mathbf{q}_1),...,\mathbf{D}_m(\mathbf{q}_m)\right]\in\Re^{mn\times mn}\\&\mathbf{C}(\mathbf{q},\dot{\mathbf{q}})=blockdiag\left[\mathbf{C}_1(\mathbf{q}_1,\dot{\mathbf{q}}_1),...,\mathbf{C}_m(\mathbf{q}_m,\dot{\mathbf{q}}_m)\right]\in\Re^{mn\times mn}\\&\mathbf{G}(\mathbf{q})=\begin{bmatrix}\mathbf{G}_1^T(\mathbf{q}_1) & \dots & \mathbf{G}_m^T(\mathbf{q}_m)\end{bmatrix}^T\in\Re^{mn}\\&\mathbf{F}_e=\begin{bmatrix}\mathbf{F}_{e1}^T & \dots & \mathbf{F}_{em}^T\end{bmatrix}^T\in\Re^{mn}\\&\mathbf{J}_e(\mathbf{q})=blockdiag\left[\mathbf{J}_{e1}(\mathbf{q}_1),...,\mathbf{J}_{em}(\mathbf{q}_m)\right]\in\Re^{mn\times mn}\end{aligned} \tag{3}$$

Without loss of generality, all the kinematic pairs of the robot are assumed further on to be revolute. Also, the following inequality holds:

$$\xi_D\mathbf{I}_{mn}\geq\mathbf{D}(\mathbf{q}),\quad\forall\mathbf{q}\in\Re^{mn} \tag{4}$$

$$\xi_C\left\|\dot{\mathbf{q}}\right\|\geq\left\|\mathbf{C}(\mathbf{q},\dot{\mathbf{q}})\right\|,\quad\forall\mathbf{q},\dot{\mathbf{q}}\in\Re^{mn} \tag{5}$$

$$\xi_G\geq\sup_{\forall\mathbf{q}\in\Re^{mn}}\left\|\mathbf{G}(\mathbf{q})\right\| \tag{6}$$

$$0<\xi_{J_e,\min}\leq\left\|\mathbf{J}_e(\mathbf{q})\right\|\leq\xi_{J_e,\max} \tag{7}$$

$$\left\|\boldsymbol{\tau}_d\right\|\leq\xi_\tau \tag{8}$$

in which $\xi_D=\lambda_{\max}(\xi_{D1},\xi_{D2},...,\xi_{Dm})$ is a positive scalar constant with ξ_{Di} denoting the maximum eigenvalue of $\mathbf{D}_i(\mathbf{q}_i)$ for i=1,..,m; $\mathbf{I}_{mn}\in\Re^{mn\times mn}$ is the identity matrix, $\xi_C=\lambda_{\max}(\xi_{C1},\xi_{C2},...,\xi_{Cm})$ is a positive scalar constant with ξ_{Ci} denoting the maximum eigenvalue of $\mathbf{C}_i(\mathbf{q}_i,\dot{\mathbf{q}}_i)$ for i=1,..,m; $\xi_{J_e,\min}=\lambda_{\min}(\xi_{J_{e1},\min},\xi_{J_{e2},\min},...,\xi_{J_{em},\min})$ and $\xi_{J_e,\max}=\lambda_{\max}(\xi_{J_{e1},\max},\xi_{J_{e2},\max},...,\xi_{J_{em},\max})$ are positive scalar constants with $\xi_{J_{ei},\min}$ and $\xi_{J_{ei},\max}$ denoting the minimum and maximum eigenvalue of $\mathbf{J}_{ei}(\mathbf{q}_i)$ for i=1,..,m, respectively. Finally ξ_G and ξ_τ are positive scalar constants.

2- 3- Modeling the Object Movement

The payload movement is modeled as [26]

$$\mathbf{D}_o(\mathbf{x}_o)\ddot{\mathbf{x}}_o+\mathbf{C}_o(\mathbf{x}_o,\dot{\mathbf{x}}_o)\dot{\mathbf{x}}_o+\mathbf{G}_o(\mathbf{x}_o)=\mathbf{F}_o \tag{9}$$

where $\mathbf{x}_o\in\Re^n$ indicates the orientation/position vector of the payload frame $O_oX_oY_oZ_o$ relative to the reference frame $OXYZ$. $\mathbf{D}_o(\mathbf{x}_o)\in\Re^{n\times n}$ is the positive-definite and symmetric payload inertial matrix. $\mathbf{G}_o(\mathbf{x}_o)\in\Re^n$ and $\mathbf{C}_o(\mathbf{x}_o,\dot{\mathbf{x}}_o)\in\Re^{n\times n}$ are the gravitational vector and the Coriolis/centrifugal forces matrix, respectively. $\mathbf{F}_o\in\Re^n$ indicates the force applied to the object's mass center and $\mathbf{J}_o(\mathbf{x}_o)$ is defined as

$$\mathbf{J}_o(\mathbf{x}_o)=\begin{bmatrix}\mathbf{J}_{o1}^T(\mathbf{x}_o) & \dots & \mathbf{J}_{om}^T(\mathbf{x}_o)\end{bmatrix}^T\in\Re^{mn\times n} \tag{10}$$

Here, $\mathbf{J}_{oi}(\mathbf{x}_o)\in\Re^{n\times n}$ represents the Jacobian matrix of the payload frame $O_oX_oY_oZ_o$ relative to the *i*th arm gripper frame $O_{ei}X_{ei}Y_{ei}Z_{ei}$. So, $\mathbf{F}_o$ is obtained as

$$\mathbf{F}_o=\mathbf{J}_o^T(\mathbf{x}_o)\mathbf{F}_e \tag{11}$$

By known consequent $\mathbf{F}_o$, the force $\mathbf{F}_e$, satisfying (11), is decomposed into two parts. These parts are orthogonal and correspond to the internal force production and the object displacement as (12) [26-27].

$$\mathbf{F}_e = \mathbf{F}_I + (\mathbf{J}_o^T(\mathbf{x}_o))^{\dagger}\mathbf{F}_o \tag{12}$$

where the pseudo-inverse of $\mathbf{J}_o^T(\mathbf{x}_o)$ is calculated as $(\mathbf{J}_o^T(\mathbf{x}_o))^{\dagger} = \mathbf{J}_o(\mathbf{x}_o)(\mathbf{J}_o^T(\mathbf{x}_o)\mathbf{J}_o(\mathbf{x}_o))^{-1} \in \Re^{mn\times n}$. Internal force $\mathbf{F}_I \in \Re^{mn}$ is described in the $\mathbf{J}_o^T(\mathbf{x}_o)$ null space. In other words, it fulfills (13).

$$\mathbf{J}_o^T(\mathbf{x}_o)\mathbf{F}_I = 0 \tag{13}$$

Integration of (12) and (9) leads to

$$\mathbf{F}_e = \mathbf{F}_I + (\mathbf{J}_o^T(\mathbf{x}_o))^{\dagger}\left(\mathbf{G}_o(\mathbf{x}_o) + \mathbf{C}_o(\mathbf{x}_o,\dot{\mathbf{x}}_o)\dot{\mathbf{x}}_o + \mathbf{D}_o(\mathbf{x}_o)\ddot{\mathbf{x}}_o\right) \tag{14}$$

The dynamic equation (9) has the following properties, which are useful for subsequent control development and analysis.

$$\xi_{D_o}\mathbf{I}_n \geq \mathbf{D}_o(\mathbf{x}_o), \quad \forall \mathbf{x}_o \in \Re^n \tag{15}$$

$$\xi_{C_o}\left\|\dot{\mathbf{x}}_o\right\| \geq \left\|\mathbf{C}_o(\mathbf{x}_o,\dot{\mathbf{x}}_o)\right\|, \quad \forall \mathbf{x}_o,\dot{\mathbf{x}}_o \in \Re^n \tag{16}$$

$$\xi_{G_o} \geq \sup_{\forall \mathbf{x}_o \in \Re^n}\left\|\mathbf{G}_o(\mathbf{x}_o)\right\| \tag{17}$$

$$0 < \sigma_{\min}(\mathbf{J}_o(\mathbf{x}_o)) \leq \left\|\mathbf{J}_o(\mathbf{x}_o)\right\| \leq \sigma_{\max}(\mathbf{J}_o(\mathbf{x}_o)) \tag{18}$$

in which ξ_{D_o}, ξ_{C_o}, and ξ_{G_o} are known positive scalar constants. Moreover, $\sigma_{\min}(\mathbf{J}_o(\mathbf{x}_o))$ and $\sigma_{\max}(\mathbf{J}_o(\mathbf{x}_o))$ are positive scalar constants representing the minimum and maximum singular value of $\mathbf{J}_o(\mathbf{x}_o)$, respectively.

2- 4- Modeling the Overall System

There are $(m+1)n$ position variables in (2) and (9), and n of them are not dependent, because the path of each robot joint is determined uniquely given a certain load path based on Assumptions 1 and 2. Due to the dependency of position variables, equations (2) and (9) are not suitable for studying system dynamics. Therefore, the independent object position $\mathbf{X}_o$ is utilized to reformulate (2), to describe the overall system behavior.

The ith robot end-effector position/orientation vector is indicated by $\mathbf{x}_{ei} \in \Re^n$. The Jacobian $\mathbf{J}_{ei}(\mathbf{q}_i)$ is then utilized to establish the equation between $\dot{\mathbf{x}}_{ei}$ and $\dot{\mathbf{q}}_i$ as (19).

$$\dot{\mathbf{x}}_{ei} = \mathbf{J}_{ei}(\mathbf{q}_i)\dot{\mathbf{q}}_i \tag{19}$$

and Eq. (20) shows the relationship between $\dot{\mathbf{x}}_{ei}$ and $\dot{\mathbf{x}}_o$.

$$\dot{\mathbf{x}}_{ei} = \mathbf{J}_{oi}(\mathbf{x}_o)\dot{\mathbf{x}}_o \tag{20}$$

Combining Equations (19) and (20) yields the following equation linking the joint velocity of the ith arm to the payload velocity:

$$\dot{\mathbf{q}}_i = \mathbf{J}_{ei}^{-1}(\mathbf{q}_i)\mathbf{J}_{oi}(\mathbf{x}_o)\dot{\mathbf{x}}_o \tag{21}$$

Since the arms move in a non-singular space, there is the inverse matrix of $\mathbf{J}_{ei}(\mathbf{q}_i)$. The robots are supposed to act on the payload at the same time. That's why,

$$\dot{\mathbf{q}} = \mathbf{J}_e^{-1}(\mathbf{q})\mathbf{J}_o(\mathbf{x}_o)\dot{\mathbf{x}}_o \tag{22}$$

Differentiating (22) leads to

$$\ddot{\mathbf{q}} = \mathbf{J}_e^{-1}(\mathbf{q})\mathbf{J}_o(\mathbf{x}_o)\ddot{\mathbf{x}}_o + \frac{d}{dt}(\mathbf{J}_e^{-1}(\mathbf{q})\mathbf{J}_o(\mathbf{x}_o))\dot{\mathbf{x}}_o \tag{23}$$

Now, utilizing equations (14), (22), and (23), the dynamic model (2) is reformulated as follows

$$\begin{aligned}&\mathbf{D}(\mathbf{q})\mathbf{J}_e^{-1}(\mathbf{q})\mathbf{J}_o(\mathbf{x}_o)\ddot{\mathbf{x}}_o\\ &+\mathbf{J}_e^T(\mathbf{q})(\mathbf{J}_o^T(\mathbf{x}_o))^{\dagger}(\mathbf{G}_o(\mathbf{x}_o)\\ &+\mathbf{D}_o(\mathbf{x}_o)\ddot{\mathbf{x}}_o + \mathbf{C}_o(\mathbf{x}_o,\dot{\mathbf{x}}_o)\dot{\mathbf{x}}_o)\\ &+\mathbf{C}(\mathbf{q},\dot{\mathbf{q}})\mathbf{J}_e^{-1}(\mathbf{q})\mathbf{J}_o(\mathbf{x}_o)\dot{\mathbf{x}}_o\\ &+\mathbf{D}(\mathbf{q})\frac{d}{dt}(\mathbf{J}_e^{-1}(\mathbf{q})\mathbf{J}_o(\mathbf{x}_o))\dot{\mathbf{x}}_o\\ &+\mathbf{G}(\mathbf{q}) = \boldsymbol{\tau} - \mathbf{J}_e^T(\mathbf{q})\mathbf{F}_I + \boldsymbol{\tau}_d\end{aligned} \tag{24}$$

Multiplying both sides of Equation (24) by $\mathbf{J}_o^T(\mathbf{x}_o)\mathbf{J}_e^{-T}(\mathbf{q})$

, and using the fact that $\mathbf{J}_o^T(\mathbf{x}_o)\mathbf{F}_I = 0$, the overall dynamics of the robotic system consisting of the payload and multiple arms, is rewritten as

$$\mathbf{M}_c(\mathbf{x}_o)\ddot{\mathbf{x}}_o + \mathbf{G}_c(\mathbf{x}_o) + \mathbf{C}_c(\mathbf{x}_o, \dot{\mathbf{x}}_o)\dot{\mathbf{x}}_o = \mathbf{u} \tag{25}$$

where

$$\begin{aligned}
&\mathbf{M}_c(\mathbf{x}_o) = \mathbf{D}_o(\mathbf{x}_o) + \\
&\mathbf{J}_o^T(\mathbf{x}_o)\mathbf{J}_e^{-T}(\mathbf{q})\mathbf{D}(\mathbf{q})\mathbf{J}_e^{-1}(\mathbf{q})\mathbf{J}_o(\mathbf{x}_o) \in \Re^{n\times n} \\
&\mathbf{C}_c(\mathbf{x}_o, \dot{\mathbf{x}}_o) = \mathbf{C}_o(\mathbf{x}_o, \dot{\mathbf{x}}_o) \\
&+\mathbf{J}_o^T(\mathbf{x}_o)\mathbf{J}_e^{-T}(\mathbf{q})(\mathbf{D}(\mathbf{q})\frac{d}{dt}(\mathbf{J}_e^{-1}(\mathbf{q})\mathbf{J}_o(\mathbf{x}_o)) \\
&+\mathbf{C}(\mathbf{q}, \dot{\mathbf{q}})\mathbf{J}_e^{-1}(\mathbf{q})\mathbf{J}_o(\mathbf{x}_o)) \in \Re^{n\times n} \\
&\mathbf{G}_c(\mathbf{x}_o) = \mathbf{G}_o(\mathbf{x}_o) \\
&+\mathbf{J}_o^T(\mathbf{x}_o)\mathbf{J}_e^{-T}(\mathbf{q})(\mathbf{G}(\mathbf{q}) - \boldsymbol{\tau}_d) \in \Re^n \\
&\mathbf{u} = \mathbf{J}_o^T(\mathbf{x}_o)\mathbf{J}_e^{-T}(\mathbf{q})\boldsymbol{\tau} \in \Re^n
\end{aligned}$$

Below, the useful properties of Equation (25) are summarized which will be utilized for designing the controller.

Property 1: $\mathbf{M}_c(\mathbf{x}_o)$ is positive-definite, which is also symmetric regarding all values of $\mathbf{x}_o$. It is also bounded from above and below, i.e., $\xi_m \mathbf{I}_n \le \mathbf{M}_c(\mathbf{x}_o) \le \xi_M \mathbf{I}_n$, where the positive constants ξ_m and ξ_M are belong to $\Re$.

Property 2: $\dot{\mathbf{M}}_c(\mathbf{x}_o) - 2\mathbf{C}_c(\mathbf{x}_o, \dot{\mathbf{x}}_o)$ satisfies the subsequent skew-symmetric equality [29].

$$\varsigma(\dot{\mathbf{M}}_c(\mathbf{x}_o) - 2\mathbf{C}_c(\mathbf{x}_o, \dot{\mathbf{x}}_o))\varsigma = 0, \qquad \forall \varsigma \in \Re$$

3- Linear PID Controller Design

3- 1- Control Law and Error Dynamics

According to (25), the mathematical model of cooperative robots contains complicated matrices that will impose difficulties on the control system and reduce its capabilities. Moreover, increasing the number of collaborative robots and their relevant degree of freedom, make the above difficulty more hypersensitive. Therefore, the control objective is to adjust the object's mass center to track a predefined trajectory in the presence of external disturbances and without any knowledge of the system's dynamic. Let us introduce the object orientation/position and its velocity tracking error as (26) with $\mathbf{x}_{od}(t) \in \Re^n$ denoting the vector of the desired orientation/position trajectory of the object.

$$\begin{aligned}
\mathbf{e}_o(t) &= \mathbf{x}_{od}(t) - \mathbf{x}_o(t), \\
\dot{\mathbf{e}}_o(t) &= \dot{\mathbf{x}}_{od}(t) - \dot{\mathbf{x}}_o(t)
\end{aligned} \tag{26}$$

Assumption 5: The desired trajectory signals $\ddot{\mathbf{x}}_{od}(t)$ and $\dot{\mathbf{x}}_{od}(t)$ are limited by A_M and V_M, respectively, i.e.,

$$A_M = \sup_t \|\ddot{\mathbf{x}}_{od}(t)\|, \qquad V_M = \sup_t \|\dot{\mathbf{x}}_{od}(t)\| \tag{27}$$

The control input is now introduced as:

$$\mathbf{u}(t) = \boldsymbol{\kappa}_d \dot{\mathbf{e}}_o(t) + \boldsymbol{\kappa}_p \mathbf{e}_o(t) + \boldsymbol{\kappa}_I \int_0^t \mathbf{e}_o(s)ds \tag{28}$$

where the $n\times n$ matrices $\boldsymbol{\kappa}_p$, $\boldsymbol{\kappa}_I$, and $\boldsymbol{\kappa}_d$ are diagonal and positive definite. Substituting Eq. (28) into the robot dynamic model (25), adding $\mathbf{M}_c(\mathbf{x}_o)\ddot{\mathbf{x}}_{od}$ to both sides of the resulted equation, using definition (26), and reorganizing with some manipulation; the closed-loop error equation of the robotic system can be shown as follows

$$\begin{aligned}
\ddot{\mathbf{e}}_o(t) = &-\mathbf{M}_c^{-1}(\mathbf{x}_o)\boldsymbol{\kappa}_d \dot{\mathbf{e}}_o(t) \\
&-\mathbf{M}_c^{-1}(\mathbf{x}_o)\boldsymbol{\kappa}_p \mathbf{e}_o(t) \\
&-\mathbf{M}_c^{-1}(\mathbf{x}_o)\boldsymbol{\kappa}_I \int_0^t \mathbf{e}_o(s)ds \\
&+\mathbf{M}_c^{-1}(\mathbf{x}_o)(\mathbf{C}_c(\mathbf{x}_o, \dot{\mathbf{x}}_o)\dot{\mathbf{x}}_o \\
&+\mathbf{G}_c(\mathbf{x}_o) + \mathbf{M}_c(\mathbf{x}_o)\ddot{\mathbf{x}}_{od})
\end{aligned} \tag{29}$$

Introducing the variable $\mathbf{y}(t)$ as

$$\mathbf{y}(t) = \begin{bmatrix} \int_0^t \mathbf{e}_o^T(s) & \mathbf{e}_o^T(s) & \dot{\mathbf{e}}_o^T(s) \end{bmatrix}^T \in \Re^{3n} \tag{30}$$

The state-space representation of the dynamical equation (29) can be obtained as follows

$$\dot{\mathbf{y}}(t) = \mathbf{A}(\mathbf{x}_o)\mathbf{y}(t) + \mathbf{B}(\mathbf{x}_o)\boldsymbol{\Delta}(t) \tag{31}$$

where the nonlinear time-varying matrices $\mathbf{A}(\mathbf{x}_o)$ and $\mathbf{B}(\mathbf{x}_o)$ are defined as

$$\mathbf{A}(\mathbf{x}_o)=\begin{bmatrix}\mathbf{0}_n & \mathbf{I}_n & \mathbf{0}_n\\ \mathbf{0}_n & \mathbf{0}_n & \mathbf{I}_n\\ -\mathbf{M}_c^{-1}(\mathbf{x}_o)\boldsymbol{\kappa}_I & -\mathbf{M}_c^{-1}(\mathbf{x}_o)\boldsymbol{\kappa}_p & -\mathbf{M}_c^{-1}(\mathbf{x}_o)\boldsymbol{\kappa}_d\end{bmatrix}\in\Re^{3n\times 3n},$$
$$\mathbf{B}(\mathbf{x}_o)=\begin{bmatrix}\mathbf{0}_n\\ \mathbf{0}_n\\ \mathbf{M}_c^{-1}(\mathbf{x}_o)\end{bmatrix}\in\Re^{3n\times n} \quad (32)$$

with

$$\boldsymbol{\Delta}(t)=\mathbf{G}_c(\mathbf{x}_o)+\mathbf{C}_c(\mathbf{x}_o,\dot{\mathbf{x}}_o)\dot{\mathbf{x}}_o+\mathbf{M}_c(\mathbf{x}_o)\ddot{\mathbf{x}}_{od}\in\Re^n \quad (33)$$

indicating the lumped sum of nonlinearities.

Remark 1: It is considerable that the actual control input applied for controlling the system is the torque vector τ. The control rule (28) should be then presented as (34) to achieve this goal.

$$\mathbf{J}_e^{-T}(\mathbf{q})\boldsymbol{\tau}=\mathbf{F}_{Ic}+(\mathbf{J}_o^T(\mathbf{x}_o))^{\dagger}\mathbf{u} \quad (34)$$

where $\mathbf{F}_{Ic}\in\Re^{mn}$ indicates the internal force control law, given by

$$\mathbf{F}_{Ic}=\mathbf{K}_I(\mathbf{F}_{Id}-\mathbf{F}_I)+\mathbf{F}_{Id} \quad (35)$$

where the gain matrix $0<\mathbf{K}_I\in\Re^{mn\times mn}$ is in diagonal form. Note that $\mathbf{F}_{Id}$ is in $\mathbf{J}_o^T(\mathbf{x}_o)$ null space, and so is $\mathbf{F}_{Ic}$.

3- 2- Stability analysis

Define

$$V(\mathbf{y})=\mathbf{y}^T\mathbf{P}\mathbf{y} \quad (36)$$

where

$$\mathbf{P}=\frac{1}{2}\begin{bmatrix}\mu\boldsymbol{\kappa}_p+\mu\boldsymbol{\kappa}_I+\mu^2\mathbf{M}_c & \mu\boldsymbol{\kappa}_d+\boldsymbol{\kappa}_I+\mu^2\mathbf{M}_c & \mu\mathbf{M}_c\\ \mu\boldsymbol{\kappa}_d+\boldsymbol{\kappa}_I+\mu^2\mathbf{M}_c & \mu\boldsymbol{\kappa}_d+\boldsymbol{\kappa}_p+\mu^2\mathbf{M}_c & \mu\mathbf{M}_c\\ \mu\mathbf{M}_c & \mu\mathbf{M}_c & \mathbf{M}_c\end{bmatrix}\in\Re^{3n\times 3n} \quad (37)$$

For the convenience of further considerations, the argument of $\mathbf{M}_c$ has been omitted. The Lyapunov function (36) is positive definite if the matrix $\mathbf{P}$ is positive definite. A proof that (37) is positive definite is given as follows. Assume that the PID controller parameters are as follows.

$$\begin{aligned}\boldsymbol{\kappa}_p&=diag(\kappa_{p1},...,\kappa_{pn})\in\Re^{n\times n},\\ \boldsymbol{\kappa}_I&=diag(\kappa_{I1},...,\kappa_{In})\in\Re^{n\times n},\\ \boldsymbol{\kappa}_d&=diag(\kappa_{d1},...,\kappa_{dn})\in\Re^{n\times n}\end{aligned} \quad (38)$$

The following lemma concludes the positive definiteness of matrix $\mathbf{P}$.

Lemma 1: Assume the following inequalities hold

$$0<\mu<0.5 \quad (39)$$

$$s_1=\mu(\lambda_{\min}(\boldsymbol{\kappa}_p)-\lambda_{\max}(\boldsymbol{\kappa}_d))-\mu\xi_M-(1-\mu)\lambda_{\max}(\boldsymbol{\kappa}_I)>0 \quad (40)$$

$$s_2=\lambda_{\min}(\boldsymbol{\kappa}_p)-\mu\xi_M-\lambda_{\max}(\boldsymbol{\kappa}_I)>0 \quad (41)$$

Hence, the matrix $\mathbf{P}$ is positive definite satisfying the following inequality:

$$\lambda_{\max}(\mathbf{P})\|\mathbf{y}\|^2\geq\mathbf{y}^T\mathbf{P}\mathbf{y}\geq\lambda_{\min}(\mathbf{P})\|\mathbf{y}\|^2 \quad (42)$$

Where

$$\lambda_{\max}(\mathbf{P})=\max\{\frac{1+2\mu}{2}\xi_M,\frac{s_3}{2},\frac{s_4}{2}\} \quad (43)$$

$$\lambda_{\min}(\mathbf{P})=\min\{\frac{1-2\mu}{2}\xi_m,\frac{s_1}{2},\frac{s_2}{2}\} \quad (44)$$

and

$$\begin{aligned}s_3&=(1+\mu)\lambda_{\max}(\boldsymbol{\kappa}_I)+\\ &\mu(\lambda_{\max}(\boldsymbol{\kappa}_p)+\lambda_{\max}(\boldsymbol{\kappa}_d))+(1+2\mu)\mu\xi_M\end{aligned} \quad (45)$$

$$\begin{aligned}s_4&=\lambda_{\max}(\boldsymbol{\kappa}_p)+2\mu\lambda_{\max}(\boldsymbol{\kappa}_d)\\ &+\lambda_{\max}(\boldsymbol{\kappa}_I)+(1+2\mu)\mu\xi_M\end{aligned} \quad (46)$$

Proof: see Appendix I.

Differentiating (36) and utilizing (31), one obtains

$$\dot{V}(\mathbf{y}) = \mathbf{y}^T(\mathbf{A}^T\mathbf{P} + \mathbf{P}\mathbf{A})\mathbf{y} + 2\mathbf{y}^T\mathbf{P}\mathbf{B}\boldsymbol{\Delta}(t) + \mathbf{y}^T\dot{\mathbf{P}}\mathbf{y} \tag{47}$$

Substituting $\mathbf{P}$ from (37) into (47) and considering property 2 one obtains

$$\begin{aligned}\dot{V}(\mathbf{y}) = &-\mathbf{y}^T\mathbf{H}\mathbf{y} + \\ &\mathbf{y}^T\mathbf{Q}_1\begin{bmatrix}\mathbf{M}_c & \mathbf{0}_n & \mathbf{0}_n\\ \mathbf{0}_n & \mathbf{M}_c & \mathbf{0}_n\\ \mathbf{0}_n & \mathbf{0}_n & \mathbf{M}_c\end{bmatrix}\mathbf{y} + \\ &\mathbf{y}^T\begin{bmatrix}\mu\mathbf{I}_n\\ \mu\mathbf{I}_n\\ \mathbf{I}_n\end{bmatrix}\boldsymbol{\Delta}(t) \\ &+\mathbf{y}^T\begin{bmatrix}\mu\mathbf{I}_n\\ \mu\mathbf{I}_n\\ \mathbf{I}_n\end{bmatrix}\mathbf{C}_c(\mathbf{x}_o,\dot{\mathbf{x}}_o)\begin{bmatrix}\mu\mathbf{I}_n & \mu\mathbf{I}_n & \mathbf{I}_n\end{bmatrix}\mathbf{y}\end{aligned} \tag{48}$$

where

$$\mathbf{H} = \begin{bmatrix}\mu\boldsymbol{\kappa}_I & \mathbf{0}_n & \mathbf{0}_n\\ \mathbf{0}_n & (\mu\boldsymbol{\kappa}_p - \mu\boldsymbol{\kappa}_d - \boldsymbol{\kappa}_I) & \mathbf{0}_n\\ \mathbf{0}_n & \mathbf{0}_n & \boldsymbol{\kappa}_d\end{bmatrix} \in \Re^{3n\times 3n} \tag{49}$$

$$\mathbf{Q}_1 = \frac{1}{2}\begin{bmatrix}\mathbf{0}_n & \mu^2\mathbf{I}_n & \mu^2\mathbf{I}_n\\ \mu^2\mathbf{I}_n & 2\mu^2\mathbf{I}_n & (\mu^2+\mu)\mathbf{I}_n\\ \mu^2\mathbf{I}_n & (\mu^2+\mu)\mathbf{I}_n & 2\mu\mathbf{I}_n\end{bmatrix} \in \Re^{3n\times 3n} \tag{50}$$

Equation (48) can also be represented as follows

$$\begin{aligned}\dot{V}(\mathbf{y}) \le &-\lambda_{\min}(\mathbf{H})\|\mathbf{y}\|^2 + \lambda_{\max}(\mathbf{Q}_1)\xi_M\|\mathbf{y}\|^2 \\ &+\lambda_{\max}(\mathbf{Q}_2)\|\mathbf{y}\|^2\|\mathbf{C}_c(\mathbf{x}_o,\dot{\mathbf{x}}_o)\| \\ &+\mu^{-1}\lambda_{\max}(\mathbf{Q}_2)\|\mathbf{y}\|\|\boldsymbol{\Delta}(t)\|\end{aligned} \tag{51}$$

in which

$$\mathbf{Q}_2 = \begin{bmatrix}\mu^2\mathbf{I}_n & \mu^2\mathbf{I}_n & \mu\mathbf{I}_n\\ \mu^2\mathbf{I}_n & \mu^2\mathbf{I}_n & \mu\mathbf{I}_n\\ \mu\mathbf{I}_n & \mu\mathbf{I}_n & \mathbf{I}_n\end{bmatrix} \in \Re^{3n\times 3n} \tag{52}$$

The last term of inequality (51) is investigated in the remaining part of this proof. It is straightforward to show that the inequality (53) is held (see Appendix II).

$$\|\boldsymbol{\Delta}(t)\| \le \beta_0 + 2L_0V_M\|\mathbf{y}(t)\| + L_0\|\mathbf{y}(t)\|^2 \tag{53}$$

where we have utilized the inequality $\|\dot{\mathbf{e}}_o(t)\| \le \|\mathbf{y}(t)\|$ and

$$\|\dot{\mathbf{x}}_o(t)\| \le V_M + \|\mathbf{y}(t)\| \tag{54}$$

$$\|\dot{\mathbf{q}}\| \le \frac{\sigma_{\max}(\mathbf{J}_o(\mathbf{x}_o))}{\xi_{J_e,\min}}\|\dot{\mathbf{x}}_o(t)\| \tag{55}$$

Replacing (53), (54), and (B3) into (51) with some further manipulation, $\dot{V}(\mathbf{y})$ is bounded as

$$\dot{V}(\mathbf{y}) \le \|\mathbf{y}\|(\psi_0 - \psi_1\|\mathbf{y}\| + \psi_2\|\mathbf{y}\|^2) \tag{56}$$

in which

$$\begin{aligned}\psi_2 &= \lambda_{\max}(\mathbf{Q}_2)L_0 + \mu^{-1}\lambda_{\max}(\mathbf{Q}_2)L_0\\ \psi_1 &= \lambda_{\min}(\mathbf{H}) - \lambda_{\max}(\mathbf{Q}_1)\xi_M\\ &\quad -\lambda_{\max}(\mathbf{Q}_2)L_0V_M - 2\mu^{-1}L_0V_M\lambda_{\max}(\mathbf{Q}_2)\\ \psi_0 &= \mu^{-1}\lambda_{\max}(\mathbf{Q}_2)\beta_0\end{aligned} \tag{57}$$

The following theorem formulates our main result.

Theorem 1: Consider the robotic system (25). The control input is designed as (28). Therefore, the controlled system error signals with the initial condition $\mathbf{y}_0$ are assured to be uniformly ultimately bounded with respect to $\mho(0,\varpi)$, provided that

$$\psi_1 > 2\sqrt{\psi_0\psi_2} \tag{58}$$

$$\psi_1^2 + \psi_1\sqrt{\psi_1^2 - 4\psi_0\psi_2} > 2\psi_0\psi_2\left(1 + \sqrt{\frac{\lambda_{\max}(\mathbf{P})}{\lambda_{\min}(\mathbf{P})}}\right) \tag{59}$$

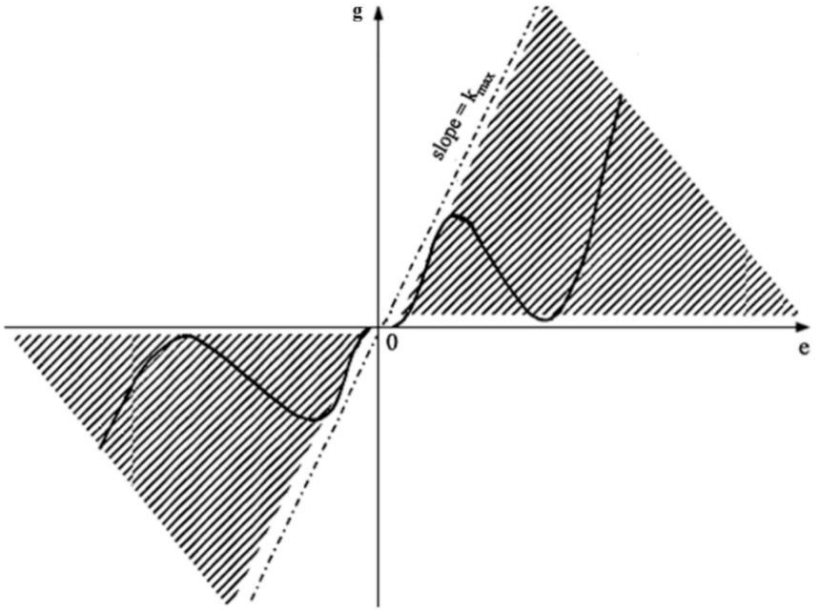

Fig. 2. Input-output characteristic of $\mathbf{k}(\mathbf{e}_o)$

$$\psi_1 + \sqrt{\psi_1^2 - 4\psi_0\psi_2} > 2\psi_2 \|\mathbf{y}_0\| \sqrt{\frac{\lambda_{\max}(\mathbf{P})}{\lambda_{\min}(\mathbf{P})}} \tag{60}$$

and

$$\varpi = \frac{2\psi_0}{\psi_1 + \sqrt{\psi_1^2 - 4\psi_0\psi_2}} \sqrt{\frac{\lambda_{\max}(\mathbf{P})}{\lambda_{\min}(\mathbf{P})}} \tag{61}$$

Proof: The proof is straightforward according to Lemma 3.5 of ref [30], (42), and (56). It is important to note that, increasing ψ_1, by proper selection of the PID control coefficients guarantees the intended conditions (58) to (60), and this completes the proof.

The boundedness of $\mathbf{y}$ implies boundedness of $\mathbf{e}_o(t)$, $\dot{\mathbf{e}}_o(t)$, and the control signal $\mathbf{u}$. Utilizing Assumption 5; $\mathbf{x}_o(t)$ and $\dot{\mathbf{x}}_o(t)$ are also bounded. These results combined with (29) obtain boundedness of $\ddot{\mathbf{x}}_o(t)$. The subsequent equation, achieved from (24), (25), and (34) presents that errors of internal force are also limited.

$$\begin{aligned}(\mathbf{F}_I - \mathbf{F}_{Id}) = -(\mathbf{I}_n + \mathbf{K}_I)^{-1} \\ \{(\mathbf{J}_o^T(\mathbf{x}_o))^+ (\mathbf{G}_c(\mathbf{x}_o) + \mathbf{M}_c(\mathbf{x}_o)\ddot{\mathbf{x}}_o \\ -\mathbf{u} + \mathbf{C}_c(\mathbf{x}_o, \dot{\mathbf{x}}_o)\dot{\mathbf{x}}_o)\}\end{aligned} \tag{62}$$

The force error is obvious to be limited and inversely proportional to $(\mathbf{I}_n + \mathbf{K}_I)$. By choosing a sufficiently large gain $\mathbf{K}_I$, the error of internal forces can be diminished to a desired small amount.

4- Nonlinear PID Controller Design

4- 1- Control law and Error Dynamics

A simple nonlinear PID controller consisting of a linear fixed PID controller in cascade with a sector-limited nonlinear gain is proposed in this paper. The control input is now introduced as

$$\mathbf{u}(t) = \bar{\boldsymbol{\kappa}}_p \mathbf{g}(t) + \bar{\boldsymbol{\kappa}}_I \int_0^t \mathbf{g}(s)ds + \bar{\boldsymbol{\kappa}}_d \frac{d}{dt}\mathbf{g}(t) \tag{63}$$

where $\mathbf{g}(t) = \mathbf{k}(\mathbf{e}_o)\mathbf{e}_o(t) \in \Re^n$ is called the scaled position error, $\mathbf{e}_o(t)$ is defined as (26), and

$$\begin{aligned}\bar{\boldsymbol{\kappa}}_p &= diag(\bar{\kappa}_{p1}, ..., \bar{\kappa}_{pn}), \\ \bar{\boldsymbol{\kappa}}_I &= diag(\bar{\kappa}_{I1}, ..., \bar{\kappa}_{In}), \\ \bar{\boldsymbol{\kappa}}_d &= diag(\bar{\kappa}_{d1}, ..., \bar{\kappa}_{dn})\end{aligned} \tag{64}$$

represent the positive constant and diagonal gain matrices.

Remark 2: The matrix $\mathbf{k}(\mathbf{e}_o) \in \Re^{n\times n}$ is diagonal and represents any sector bounded nonlinear function satisfying $\mathbf{0}_n \le \mathbf{k}(\mathbf{e}_o) \le k_{\max}\mathbf{I}_n$. Fig. 2 shows the input-output characteristics of $\mathbf{k}(\mathbf{e}_o)$; showing that the output $\mathbf{g}(t)$ lies within the shaded area $k_{\max}\|\mathbf{e}_o(t)\| \ge \|\mathbf{g}(t)\| \ge 0$.

Remark 3: Assume that, the nonlinear gain $\mathbf{k}(\mathbf{e}_o)$ is a hyperbolic secant function with respect to the object's mass center position error $\mathbf{e}_o(t)$, i.e.,

$$\mathbf{k}(\mathbf{e}_o) = \mathbf{k}_0 + \mathbf{k}_1\{\mathbf{I}_n - \mathrm{sech}(\mathbf{e}_o)\} \tag{65}$$

where $\mathbf{k}_0$ and $\mathbf{k}_1$ are the $n\times n$ constant and positive diagonal matrices; $\text{sech}(\mathbf{e}_o) = diag\,(\text{sech}(e_{o,1}),...,\text{sech}(e_{o,n}))$ with $\text{sech}(e_{o,i}) = \dfrac{2}{\exp(e_{o,i}) + \exp(-e_{o,i})}$ and $e_{o,i} \in \Re$ for i=1,...,n . As a result, $\mathbf{k}(\mathbf{e}_o)$ is limited by $k_{\max} = k_0 + k_1$ from above with k_0 and k_1 denoting the maximum eigenvalues of $\mathbf{k}_0$ and $\mathbf{k}_1$, respectively. The lower bound of the gain matrix $\mathbf{k}(\mathbf{e}_o)$ is also given by k_0 when $\mathbf{e}_o = 0$.

Substituting (63) into (25), using definitions $\mathbf{g}(t)$, (26), (30), and (65), and rearranging with some manipulation leads to

$$\dot{\mathbf{y}}(t) = \bar{\mathbf{A}}(\mathbf{x}_o)\mathbf{y}(t) + \bar{\mathbf{B}}(\mathbf{x}_o)\bar{\boldsymbol{\Delta}}(t) \tag{66}$$

in which

$$\mathbf{A}(\mathbf{x}_o) = \begin{bmatrix} \mathbf{0}_n & \mathbf{I}_n & \mathbf{0}_n \\ \mathbf{0}_n & \mathbf{0}_n & \mathbf{I}_n \\ -\mathbf{M}_c^{-1}(\mathbf{x}_o)\boldsymbol{\Gamma}_I & -\mathbf{M}_c^{-1}(\mathbf{x}_o)\boldsymbol{\Gamma}_p & -\mathbf{M}_c^{-1}(\mathbf{x}_o)\boldsymbol{\Gamma}_d \end{bmatrix} \in \Re^{3n\times 3n}, \quad \mathbf{B}(\mathbf{x}_o) = \begin{bmatrix} \mathbf{0}_n \\ \mathbf{0}_n \\ \mathbf{M}_c^{-1}(\mathbf{x}_o) \end{bmatrix} \in \Re^{3n\times n} \tag{67}$$

with

$$\begin{aligned} \bar{\boldsymbol{\Delta}}(t) = \{&\mathbf{M}_c(\mathbf{x}_o)\ddot{\mathbf{x}}_{od} + \mathbf{G}_c(\mathbf{x}_o) + \mathbf{C}_c(\mathbf{x}_o,\dot{\mathbf{x}}_o)\dot{\mathbf{x}}_o + \bar{\boldsymbol{\kappa}}_p\mathbf{k}_1\,\text{sech}(\mathbf{e}_o)\mathbf{e}_o \\ &+\bar{\boldsymbol{\kappa}}_I\mathbf{k}_1\int_0^t \text{sech}(\mathbf{e}_o(s))\mathbf{e}_o(s)ds + \bar{\boldsymbol{\kappa}}_d\mathbf{k}_1\,\text{sec}\,h(\mathbf{e}_o)\dot{\mathbf{e}}_o \\ &-\bar{\boldsymbol{\kappa}}_d\mathbf{k}_1\tanh(\mathbf{e}_o)\text{sech}(\mathbf{e}_o)\boldsymbol{\delta}(t)\mathbf{e}_o\} \end{aligned} \tag{68}$$

denoting the lumped sum of nonlinearities belong to $\Re^n$; $\delta(t) = diag\,(\dot{e}_{o,1},\dot{e}_{o,2}...,\dot{e}_{o,n}) \in \Re^{n\times n}$; $\tanh(\mathbf{e}_o) = diag\,(\tanh(e_{o,1}),...,\tanh(e_{o,n})) \in \Re^{n\times n}$ by $\tanh(e_{o,i}) = \dfrac{\exp(e_{o,i}) - \exp(-e_{o,i})}{\exp(e_{o,i}) + \exp(-e_{o,i})}$ for $e_{o,i} \in \Re$, $\Gamma_p = \bar{\kappa}_p(k_0 + k_1)$, $\Gamma_I = \bar{\kappa}_I(k_0 + k_1)$ and $\Gamma_d = \bar{\kappa}_d(k_0 + k_1)$.

Remark 4: The matrices $\text{sec}\,h(\mathbf{e}_o)$ and $\tanh(\mathbf{e}_o)$ have maximum eigenvalues equal to one, for all $\mathbf{e}_o \in \Re^n$, i.e. [41].

4- 2- Stability analysis

The following lemma is required in the following stability analysis.

Lemma 2: Let *f* and *W* be two continuous functions on [a,b] and assume *W* is positive. Then, $\int_a^b f(\varsigma)W(\varsigma)d\varsigma = f(\xi)\int_a^b W(\varsigma)d\varsigma$ for some ξ in [a,b].

A Lyapunov function candidate is suggested as follows to enable the closed-loop system stability analysis.

$$V(\mathbf{y}) = \mathbf{y}^T\bar{\mathbf{P}}\mathbf{y} \tag{69}$$

where

$$\bar{\mathbf{P}} = \frac{1}{2}\begin{bmatrix} \bar{\mu}\boldsymbol{\Gamma}_p + \bar{\mu}\boldsymbol{\Gamma}_I + \bar{\mu}^2\mathbf{M}_c & \bar{\mu}\boldsymbol{\Gamma}_d + \boldsymbol{\Gamma}_I + \bar{\mu}^2\mathbf{M}_c & \bar{\mu}\mathbf{M}_c \\ \bar{\mu}\boldsymbol{\Gamma}_d + \boldsymbol{\Gamma}_I + \bar{\mu}^2\mathbf{M}_c & \bar{\mu}\boldsymbol{\Gamma}_d + \boldsymbol{\Gamma}_p + \bar{\mu}^2\mathbf{M}_c & \bar{\mu}\mathbf{M}_c \\ \bar{\mu}\mathbf{M}_c & \bar{\mu}\mathbf{M}_c & \mathbf{M}_c \end{bmatrix} \in \Re^{3n\times 3n} \tag{70}$$

The Lyapunov function (69) is positive definite if the matrix $\bar{\mathbf{P}}$ be positive definite. A proof that the matrix $\bar{\mathbf{P}}$ is positive definite is the same as those done in section 3.2. In other words, by choosing the control parameters as

$$\begin{aligned} \boldsymbol{\Gamma}_p &= diag\,(\Gamma_{p1},...,\Gamma_{pn}), \\ \boldsymbol{\Gamma}_I &= diag\,(\Gamma_{I1},...,\Gamma_{In}), \\ \boldsymbol{\Gamma}_d &= diag\,(\Gamma_{d1},...,\Gamma_{dn}) \end{aligned} \tag{71}$$

and assuming the following definitions and inequalities

$$0 < \bar{\mu} < 0.5 \tag{72}$$

$$\bar{s}_1 = \bar{\mu}(\lambda_{\min}(\boldsymbol{\Gamma}_p) - \lambda_{\max}(\boldsymbol{\Gamma}_d)) - (1-\bar{\mu})\lambda_{\max}(\boldsymbol{\Gamma}_I) - \bar{\mu}\xi_M > 0 \tag{73}$$

$$\bar{s}_2 = \lambda_{\min}(\boldsymbol{\Gamma}_p) - \lambda_{\max}(\boldsymbol{\Gamma}_I) - \bar{\mu}\xi_M > 0 \tag{74}$$

$$\begin{aligned} \bar{s}_3 &= (1+\bar{\mu})\lambda_{\max}(\boldsymbol{\Gamma}_I) \\ &+\bar{\mu}(\lambda_{\max}(\boldsymbol{\Gamma}_p) + \lambda_{\max}(\boldsymbol{\Gamma}_d)) + (1+2\bar{\mu})\bar{\mu}\xi_M \end{aligned} \tag{75}$$

$$\begin{aligned} \bar{s}_4 &= \lambda_{\max}(\boldsymbol{\Gamma}_p) + 2\bar{\mu}\lambda_{\max}(\boldsymbol{\Gamma}_d) \\ &+\lambda_{\max}(\boldsymbol{\Gamma}_I) + (1+2\bar{\mu})\bar{\mu}\xi_M \end{aligned} \tag{76}$$

It can be concluded the positive definiteness of matrix $\bar{\mathbf{P}}$ satisfying the inequality below

$$\lambda_{\max}(\bar{\mathbf{P}})\|\mathbf{y}\|^2 \geq \mathbf{y}^T\bar{\mathbf{P}}\mathbf{y} \geq \lambda_{\min}(\bar{\mathbf{P}})\|\mathbf{y}\|^2 \tag{77}$$

in which

$$\lambda_{\max}(\bar{\mathbf{P}}) = \max\{\frac{1+2\bar{\mu}}{2}\xi_M, \frac{\bar{s}_3}{2}, \frac{\bar{s}_4}{2}\} \tag{78}$$

$$\lambda_{\min}(\bar{\mathbf{P}}) = \min\{\frac{1-2\bar{\mu}}{2}\xi_m, \frac{\bar{s}_1}{2}, \frac{\bar{s}_2}{2}\} \tag{79}$$

Proof: the roof is the same as those done in Appendix I.

Differentiating (69) with respect to time along the trajectories of the uncertain system (66) gives

$$\dot{V}(\mathbf{y}) = \mathbf{y}^T(\bar{\mathbf{A}}^T\bar{\mathbf{P}} + \bar{\mathbf{P}}\bar{\mathbf{A}})\mathbf{y} + 2\mathbf{y}^T\bar{\mathbf{P}}\bar{\mathbf{B}}\bar{\boldsymbol{\Delta}}(t) + \mathbf{y}^T\dot{\bar{\mathbf{P}}}\mathbf{y} \tag{80}$$

Substituting $\bar{\mathbf{P}}$ from (70) into (80), utilizing the same manipulation as section 3.2, one obtains

$$\begin{aligned}\dot{V}(\mathbf{y}) \le & -\lambda_{\min}(\bar{\mathbf{H}})\|\mathbf{y}\|^2 + \lambda_{\max}(\bar{\mathbf{Q}}_1)\xi_M\|\mathbf{y}\|^2 \\ & + \lambda_{\max}(\bar{\mathbf{Q}}_2)\|\mathbf{y}\|^2\|\mathbf{C}_c(\mathbf{x}_o, \dot{\mathbf{x}}_o)\| \\ & + \bar{\mu}^{-1}\lambda_{\max}(\bar{\mathbf{Q}}_2)\|\mathbf{y}\|\|\bar{\boldsymbol{\Delta}}(t)\|\end{aligned} \tag{81}$$

where

$$\bar{\mathbf{H}} = \begin{bmatrix} \bar{\mu}\boldsymbol{\Gamma}_I & \mathbf{0}_n & \mathbf{0}_n \\ \mathbf{0}_n & (\bar{\mu}\boldsymbol{\Gamma}_p - \bar{\mu}\boldsymbol{\Gamma}_d - \boldsymbol{\Gamma}_I) & \mathbf{0}_n \\ \mathbf{0}_n & \mathbf{0}_n & \boldsymbol{\Gamma}_d \end{bmatrix} \in \Re^{3n\times 3n} \tag{82}$$

$$\bar{\mathbf{Q}}_1 = \frac{1}{2}\begin{bmatrix} \mathbf{0}_n & \bar{\mu}^2\mathbf{I}_n & \bar{\mu}^2\mathbf{I}_n \\ \bar{\mu}^2\mathbf{I}_n & 2\bar{\mu}^2\mathbf{I}_n & (\bar{\mu}^2+\bar{\mu})\mathbf{I}_n \\ \bar{\mu}^2\mathbf{I}_n & (\bar{\mu}^2+\bar{\mu})\mathbf{I}_n & 2\bar{\mu}\mathbf{I}_n \end{bmatrix} \in \Re^{3n\times 3n} \tag{83}$$

and

$$\bar{\mathbf{Q}}_2 = \begin{bmatrix} \bar{\mu}^2\mathbf{I}_n & \bar{\mu}^2\mathbf{I}_n & \bar{\mu}\mathbf{I}_n \\ \bar{\mu}^2\mathbf{I}_n & \bar{\mu}^2\mathbf{I}_n & \bar{\mu}\mathbf{I}_n \\ \bar{\mu}\mathbf{I}_n & \bar{\mu}\mathbf{I}_n & \mathbf{I}_n \end{bmatrix} \in \Re^{3n\times 3n} \tag{84}$$

According to (53), using $\|\delta(t)\| \le \|\mathbf{y}\|$ and lemma 2, it can be shown that

$$\begin{aligned}\|\bar{\boldsymbol{\Delta}}(t)\| \le & \beta_0 + \{L_0 + \lambda_{\max}(\bar{\boldsymbol{\kappa}}_d)\lambda_{\max}(\mathbf{k}_1)\}\|\mathbf{y}\|^2 \\ & + \{2L_0V_M + \lambda_{\max}(\bar{\boldsymbol{\kappa}}_p)\lambda_{\max}(\mathbf{k}_1) \\ & + \lambda_{\max}(\bar{\boldsymbol{\kappa}}_d)\lambda_{\max}(\mathbf{k}_1) \\ & + \lambda_{\max}(\bar{\boldsymbol{\kappa}}_I)\lambda_{\max}(\mathbf{k}_1)\}\|\mathbf{y}(t)\|\end{aligned} \tag{85}$$

By replacing (85), (B3), and (54) into (81), and some further simplifications, (81) is reduced to

$$\dot{V}(\mathbf{y}) \le \|\mathbf{y}\|(\bar{\psi}_0 - \bar{\psi}_1\|\mathbf{y}\| + \bar{\psi}_2\|\mathbf{y}\|^2) \tag{86}$$

in which

$$\begin{aligned}\bar{\psi}_0 &= \bar{\mu}^{-1}\lambda_{\max}(\bar{\mathbf{Q}}_2)\beta_0 \\ \bar{\psi}_1 &= \lambda_{\min}(\bar{\mathbf{H}}) - \lambda_{\max}(\bar{\mathbf{Q}}_1)\xi_M \\ &\quad - \lambda_{\max}(\bar{\mathbf{Q}}_2)L_0V_M \\ &\quad - \{2L_0V_M + \lambda_{\max}(\bar{\boldsymbol{\kappa}}_p)\lambda_{\max}(\mathbf{k}_1) \\ &\quad + \lambda_{\max}(\bar{\boldsymbol{\kappa}}_d)\lambda_{\max}(\mathbf{k}_1) \\ &\quad + \lambda_{\max}(\bar{\boldsymbol{\kappa}}_I)\lambda_{\max}(\mathbf{k}_1)\}\bar{\mu}^{-1}\lambda_{\max}(\bar{\mathbf{Q}}_2) \\ \bar{\psi}_2 &= \{L_0(1+\bar{\mu}) \\ &\quad + \lambda_{\max}(\bar{\boldsymbol{\kappa}}_d)\lambda_{\max}(\mathbf{k}_1)\}\bar{\mu}^{-1}\lambda_{\max}(\bar{\mathbf{Q}}_2)\end{aligned} \tag{87}$$

The following theorem formulates our main result.

Theorem 2: Consider the robotic system (25). The control input is designed as (63). Therefore, the controlled system error signals under initial condition $\mathbf{y}_0$ is assured to be UUB with respect to region $\mho(0, \bar{\varpi})$ provided that

$$\bar{\psi}_1 > 2\sqrt{\bar{\psi}_0\bar{\psi}_2} \tag{88}$$

$$\bar{\psi}_1^2 + \bar{\psi}_1\sqrt{\bar{\psi}_1^2 - 4\bar{\psi}_0\bar{\psi}_2} > 2\bar{\psi}_0\bar{\psi}_2\left(1 + \sqrt{\frac{\lambda_{\max}(\bar{\mathbf{P}})}{\lambda_{\min}(\bar{\mathbf{P}})}}\right) \tag{89}$$

$$\bar{\psi}_1 + \sqrt{\bar{\psi}_1^2 - 4\bar{\psi}_0\bar{\psi}_2} > 2\bar{\psi}_2\|\mathbf{y}_0\|\sqrt{\frac{\lambda_{\max}(\bar{\mathbf{P}})}{\lambda_{\min}(\bar{\mathbf{P}})}} \tag{90}$$

and

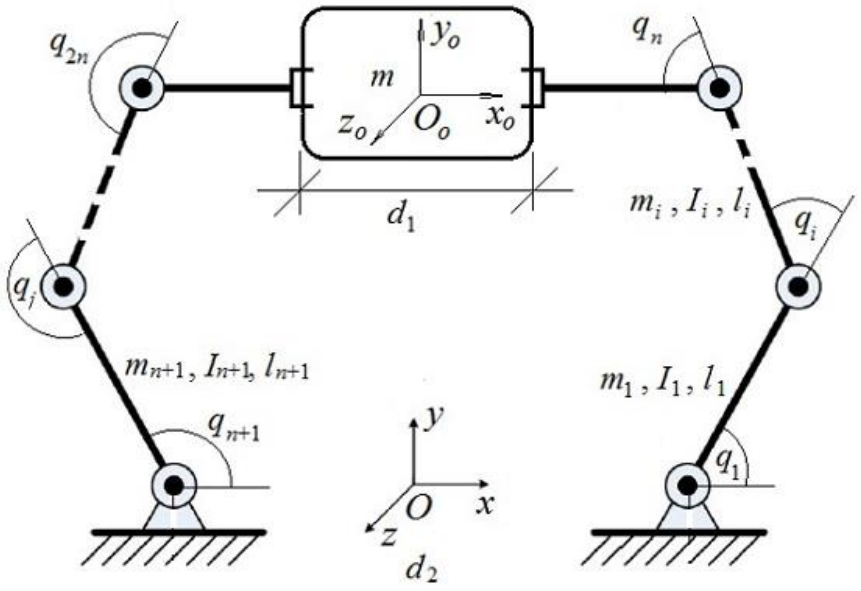

Fig. 3. Two 3-DOF cooperative manipulators [42]

$$\bar{\varpi} = \frac{2\bar{\psi}_0}{\bar{\psi}_1 + \sqrt{\bar{\psi}_1^2 - 4\bar{\psi}_0\bar{\psi}_2}} \sqrt{\frac{\lambda_{\max}(\bar{\mathbf{P}})}{\lambda_{\min}(\bar{\mathbf{P}})}} \tag{91}$$

Proof: the proof is straightforward according to Lemma 3.5 of ref [30], (77), and (86). It is useful to note that, increasing $\bar{\psi}_1$ by proper selection of the PID control coefficients guarantees the intended conditions (88) to (90), and this completes the proof.

5- Results and Discussion

A cooperating robotic system composed of two 3-DOF arms transporting an item is studied in order to apply the developed controllers (Fig 3). [37] provides details of the system modeling information (e.g., the robots' Jacobian, matrices of Coriolis and centripetal, inertia and vector of gravity terms). Throughout the simulation, the indices i=1, 2 indicates the two arms . Assume that the base frame is just in the middle of arms. Robot parameters are numerically set to $l_{1,1} = l_{2,1} = 2.05m$, $l_{1,2} = l_{2,2} = 2.05m$, and $l_{1,3} = l_{2,3} = 0.5m$ showing each link length. $m_{1,1} = m_{2,1} = 1kg$, $m_{1,2} = m_{2,2} = 1kg$, and $m_{1,3} = m_{2,3} = 0.3kg$ denote the link masses. $I_{2,1} = I_{1,1} = 0.7kgm^2$, $I_{2,2} = I_{1,2} = 0.5kgm^2$, and $I_{2,3} = I_{1,3} = 0.3kgm^2$ are moments of inertia of the links. Equation (9) gives the object dynamics, where

$$\begin{aligned} &\mathbf{D}_o(\mathbf{x}_o) = blockdiag(m_o, m_o, I_o), \\ &\mathbf{G}_o(\mathbf{x}_o) = \begin{bmatrix} 0 & m_o g & 0 \end{bmatrix}^T \end{aligned} \tag{92}$$

with I_o and m_o denoting the object's inertia and mass, respectively. Equation (10) presents the grasp matrix with

$$\mathbf{J}_{oi}(\mathbf{x}_o) = \begin{bmatrix} 1 & 0 & l_{il}\sin(x_{o3}) \\ 0 & 1 & -l_{il}\cos(x_{o3}) \\ 0 & 0 & 1 \end{bmatrix}, \quad \text{i=1,2} \tag{93}$$

In the last equation, l_{il} stands for the distance from the ith robot gripper to the object's mass center. The values of I_o and m_o parameters are chosen as 0.1kgm^2 and 0.2kg, respectively. The designing parameters for the PID and the nonlinear PID controllers have been chosen as $\kappa_p = \bar{\kappa}_p = diag(800,800,800)$, $\kappa_I = \bar{\kappa}_I = diag(100,100,100)$, $\kappa_d = \bar{\kappa}_d = diag(2,2,2)\times 10^2$, $\mathbf{k}_0 = diag(20,20,20)$, $\mathbf{k}_1 = diag(2,2,2)\times 10^2$, and $\mathbf{K}_I = diag(10^2,10^2,10^2,10^2,10^2,10^2)$.

The proposed controllers' performance is compared to the Chebyshev neural network-based (CNN) uncertainty approximator presented in [43]. The controller is given as follows

$$\boldsymbol{\tau}=\hat{\mathbf{W}}_M^T\mathbf{Z}_M\dot{\mathbf{v}}(t)+\hat{\mathbf{W}}_C^T\mathbf{Z}_C\mathbf{v}(t)+\hat{\mathbf{W}}_G^T\mathbf{Z}_G+\hat{\mathbf{W}}_\tau^T\mathbf{Z}_\tau-\mathbf{K}_D\boldsymbol{\Lambda}_\phi(\mathbf{q})\mathbf{s}(t)$$
$$+\mathbf{J}_e^T(\mathbf{q})(\mathbf{F}_{Id}(t)+\mathbf{K}_I\int_0^t(\mathbf{F}_{Id}(\varpi)-\mathbf{F}_I(\varpi))d\varpi) \quad (94)$$

where

$$\mathbf{e}_o(t)=\mathbf{x}_o(t)-\mathbf{x}_{od}(t) \quad (95)$$

$$\mathbf{s}(t)=(\dot{\mathbf{e}}_o(t)+\boldsymbol{\Lambda}\mathbf{e}_o(t))\in\Re^n \quad (96)$$

and the adaption laws are in the form of

$$\begin{aligned}\dot{\hat{\mathbf{W}}}_M&=-\mathbf{Q}_M^{-1}(\mathbf{Z}_M\dot{\mathbf{v}}(t)\mathbf{s}^T\boldsymbol{\Lambda}_\phi^T(\mathbf{q})+\sigma_M\hat{\mathbf{W}}_M)\\ \dot{\hat{\mathbf{W}}}_C&=-\mathbf{Q}_C^{-1}(\mathbf{Z}_C\mathbf{v}(t)\mathbf{s}^T\boldsymbol{\Lambda}_\phi^T(\mathbf{q})+\sigma_C\hat{\mathbf{W}}_C)\\ \dot{\hat{\mathbf{W}}}_G&=-\mathbf{Q}_G^{-1}(\mathbf{Z}_G\mathbf{s}^T\boldsymbol{\Lambda}_\phi^T(\mathbf{q})+\sigma_G\hat{\mathbf{W}}_G)\\ \dot{\hat{\mathbf{W}}}_\tau&=-\mathbf{Q}_\tau^{-1}(\mathbf{Z}_\tau\mathbf{s}^T\boldsymbol{\Lambda}_\phi^T(\mathbf{q})+\sigma_\tau\hat{\mathbf{W}}_\tau)\end{aligned} \quad (97)$$

The detailed description of CNN and its approximation properties can be found in [44]. The values of the controller parameters are similar to those presented in [43]. The first term of the Chebyshev polynomials is picked to construct the basis functions for the neural network. The initial weights of the CNN are taken to be zero. As introduced in [43], the required basis functions for nonlinear function approximation are $\mathbf{Z}_M\in\Re^{126\times3}$, $\mathbf{Z}_C\in\Re^{234\times3}$, $\mathbf{Z}_G\in\Re^{42}$, and $\mathbf{Z}_{\hat{\mathbf{0}}}\in\Re^{42}$. Suppose that the external disturbance (98) is injected to each robot manipulator.

$$\boldsymbol{\tau}_{d,i}(t)=\begin{bmatrix}2+\cos(2t) & \sin(t)+\cos(t) & 2+2\sin(2t)\end{bmatrix}^T, \quad i=1,2 \quad (98)$$

To study the controller response, two different desired trajectories are defined in the following cases.

Case 1: Consider the following path

$$\mathbf{x}_{od}(t)=\begin{bmatrix}\dfrac{0.5\cos(t+4)}{1+\sin^2(t)} & \dfrac{0.5\cos(t)\sin(t)}{1+\sin(t+4)\sin(t)}+1.65 & 0\end{bmatrix}^T \quad (99)$$

The desired value of $\mathbf{F}_{Id}(t)$ is set to zero. The initial speeds of two 3-DOF manipulators are zero for both robots and initial values of $\mathbf{q}$ is $\mathbf{q}(0)=\begin{bmatrix}-0.2272 & -2.2961 & 2.5233 & -2.5233 & 2.2961 & 3.3688\end{bmatrix}^T$. Fig. 4 shows the desired and actual coordination of the object's mass center. As can be seen, the suggested nonlinear PID controller and Chebyshev neural network-based controller are successful in tracking the reference trajectory; while the linear PID controller fails to track the reference

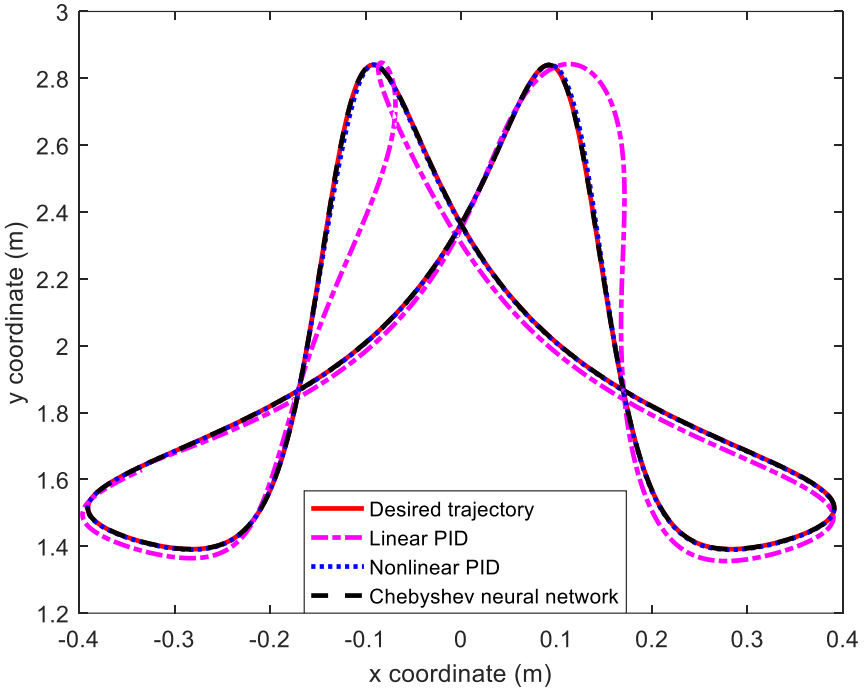

Fig. 4. Object trajectory tracking in the x-y plane

Table 1. The required parameters for implementing of three controllers

	Adjustable parameters
PID controller	$\boldsymbol{\kappa}_p$, $\boldsymbol{\kappa}_I$, $\boldsymbol{\kappa}_d$, $\mathbf{K}_I$
Nonlinear PID controller	$\bar{\boldsymbol{\kappa}}_p$, $\bar{\boldsymbol{\kappa}}_I$, $\bar{\boldsymbol{\kappa}}_d$, $\mathbf{K}_I$, $\mathbf{k}_0$, $\mathbf{k}_1$
The Chebyshev neural network-based controller	$\boldsymbol{\Lambda}$, $\mathbf{K}_D$, $\mathbf{K}_I$, $\mathbf{Q}_M \in \Re^{126\times126}$, $\mathbf{Q}_C \in \Re^{234\times234}$, $\mathbf{Q}_G \in \Re^{42\times42}$, $\mathbf{Q}_\tau \in \Re^{42\times42}$

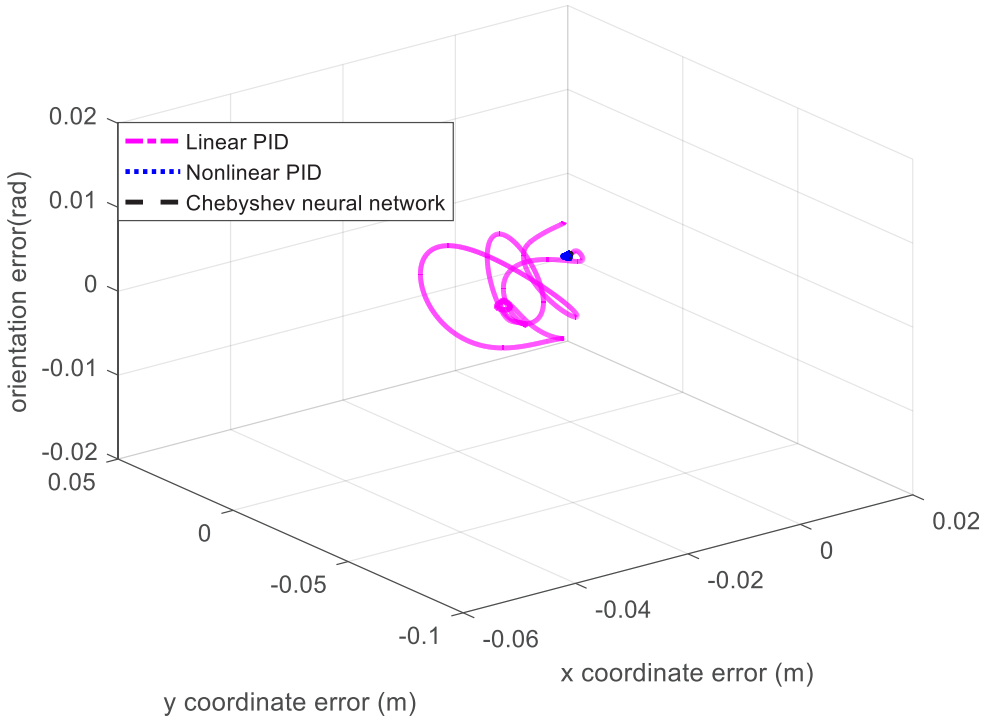

Fig. 5. Errors of orientation/position tracking

trajectory (99), under the same controller settings, initial conditions, and external disturbances. Being a single-layer neural network, the computational complexity of CNN is less intensive as compared to multi-layered perceptron (MLP) and can be used for online learning [45]. However, the proposed nonlinear PID control scheme is much simpler and less computational than CNN, since it has few tuning control parameters with low dimensions.

Table 1 compares the required controller parameters for implementing of three controllers. Fig. 5 demonstrates small and UUB tacking errors in the xy coordinates and orientation. The joint angles for both robots are given in Figs. 6 and 7. The relative control inputs applied to the robots are illustrated in Figs. 8 and 9. The results are acceptable given that the signal oscillations are diminished very quickly, and chattering does not appear in the signals. Moreover, the boundedness of the signals is maintained.

Finally, tracking of the internal force are given by Figs. 10 and 11.

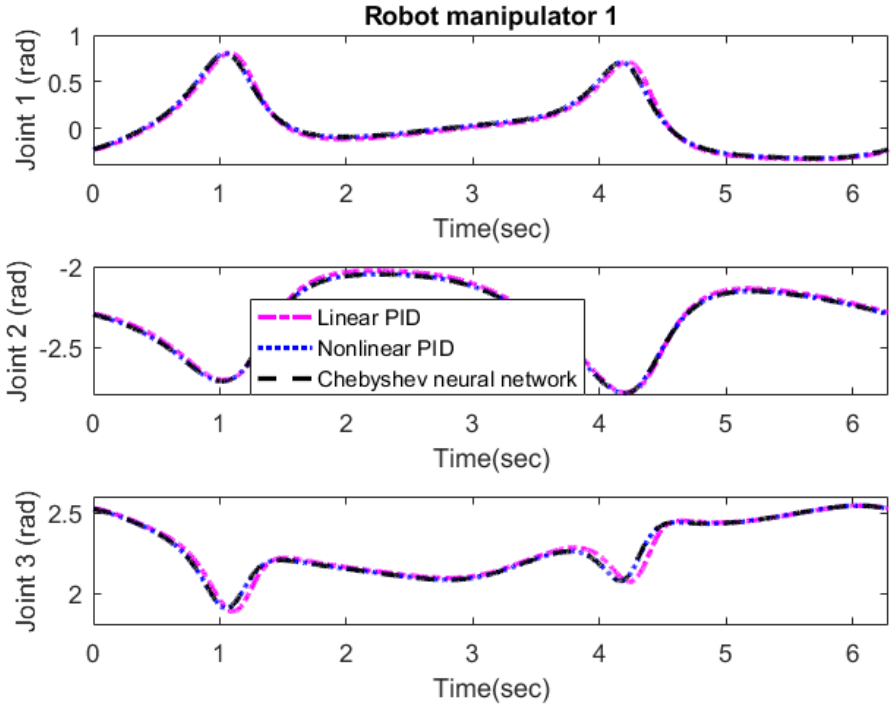

Fig. 6. First arm joints' angles

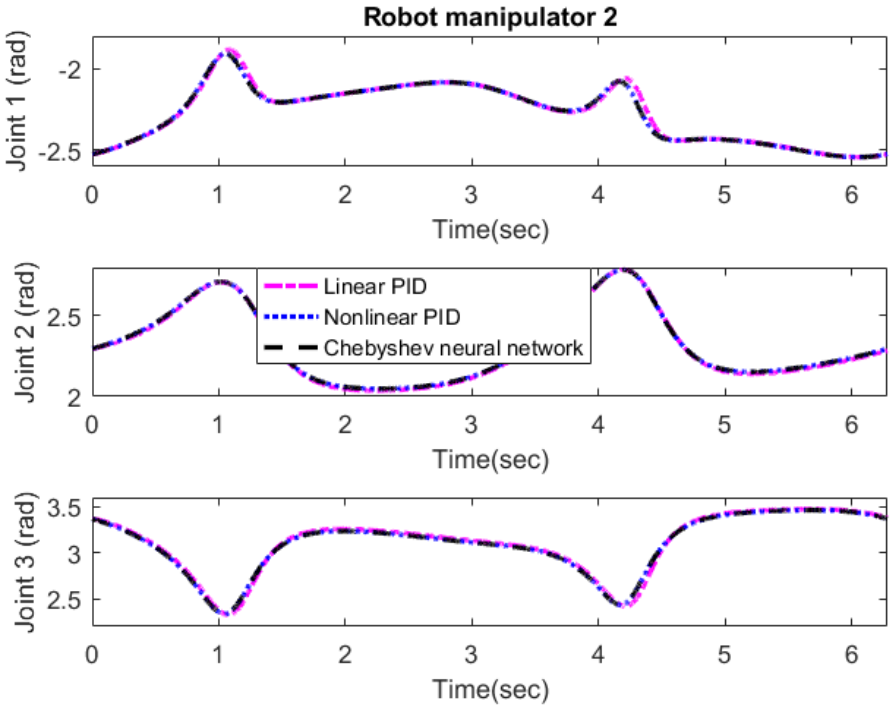

Fig. 7. Second arm joints' angles

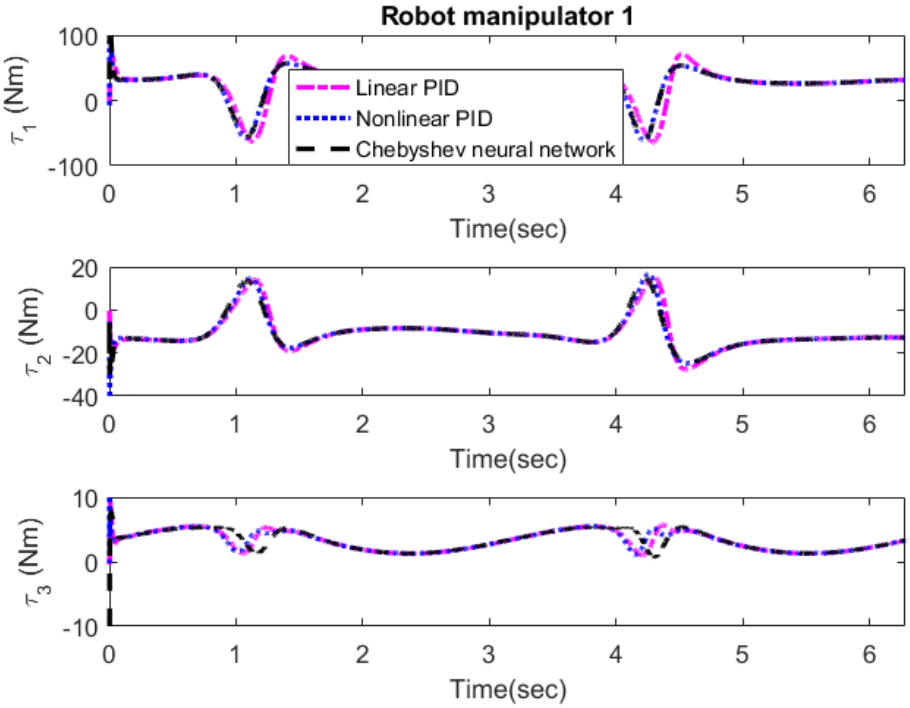

Fig. 8. Control signals applied to the first robot

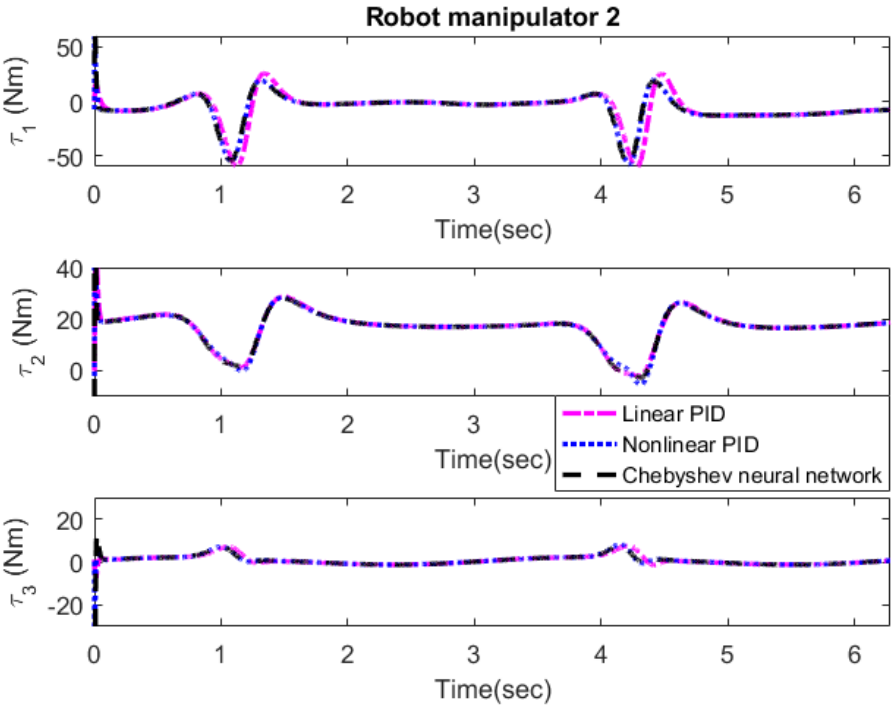

Fig. 9. Control signals applied to the second robot

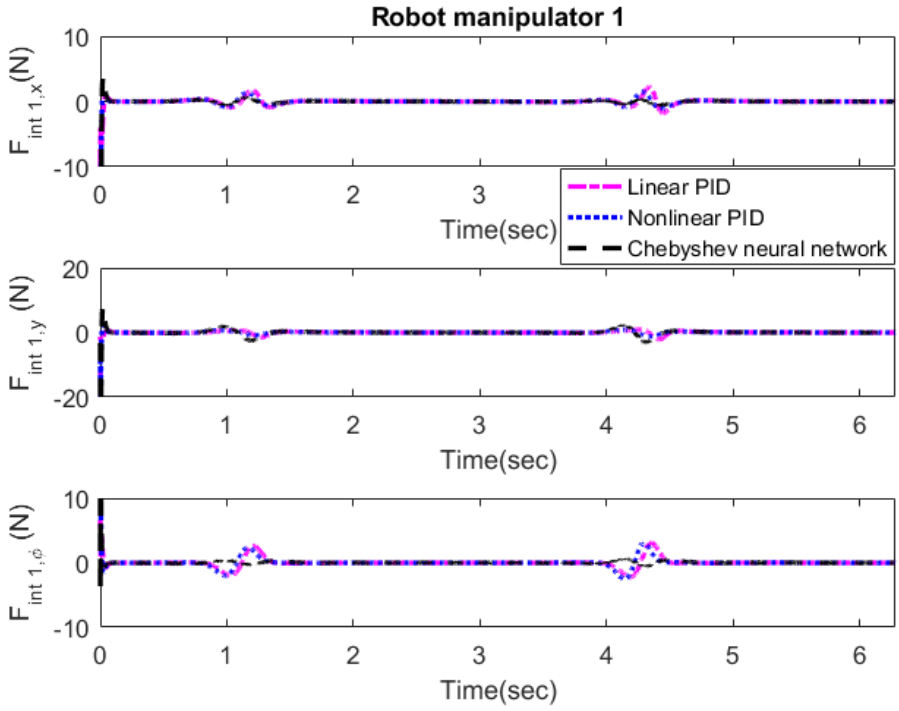

Fig. 10. First robot's internal force tracking

Case2: Consider the following desired trajectory

$$\mathbf{x}_{od}(t)=\begin{bmatrix} 0.125sin(1.1t)+0.125sin(2t) \\ 0.125sin\left(1.1t+1.6\right)+2+0.125sin\left(2t+1.6\right) \\ 0 \end{bmatrix} \quad (100)$$

In this simulation, assume that we have $\mathbf{q}(0)=\begin{bmatrix}2.5607 & -1.9798 & -0.5809 & 0.5809 & 1.9798 & 0.5809\end{bmatrix}^{\mathrm{T}}$. In this trajectory fast and complicated interactions among various dynamics of the system are inevitable. All control parameters' values are the same as before. Fig. 12 demonstrates the load's tracking in the x-y coordinate. Based on the obtained results, the proposed nonlinear PID controller and Chebyshev neural network-based controller fulfill acceptable performance for the dual-arm robotic system compared with the linear PID controller. The tracking errors along the x-y coordinate and the orientation error are illustrated in Fig. 13. The angular positions for both arms are given in Fig. 14 and Fig. 15. Control signals for this case are presented in Fig. 16 and Fig. 17. As can be seen in these figures, the control signals are limited and smooth.

or the internal forces, the tracking performances are presented in Fig. 18 and Fig. 19.

To compare the results more accurately, three performance indices are considered. The first index is the integral of squared error (ISE),

$$ISE=\int_0^t \left\|\mathbf{e}_o(\ell)\right\|^2 d\ell \quad (101)$$

The second performance index is

$$IAE=\int_0^t \left\|\mathbf{e}_o(\ell)\right\| d\ell \quad (102)$$

Finally, the third index is described as

$$ITAE=\int_0^t \ell\left\|\mathbf{e}_o(\ell)\right\| d\ell \quad (103)$$

where t is the final time defined for the simulation. Equations (101)-(103) are usual performance indices in control engineering. Based on these outcomes, the proposed nonlinear PID controller and Chebyshev neural network-

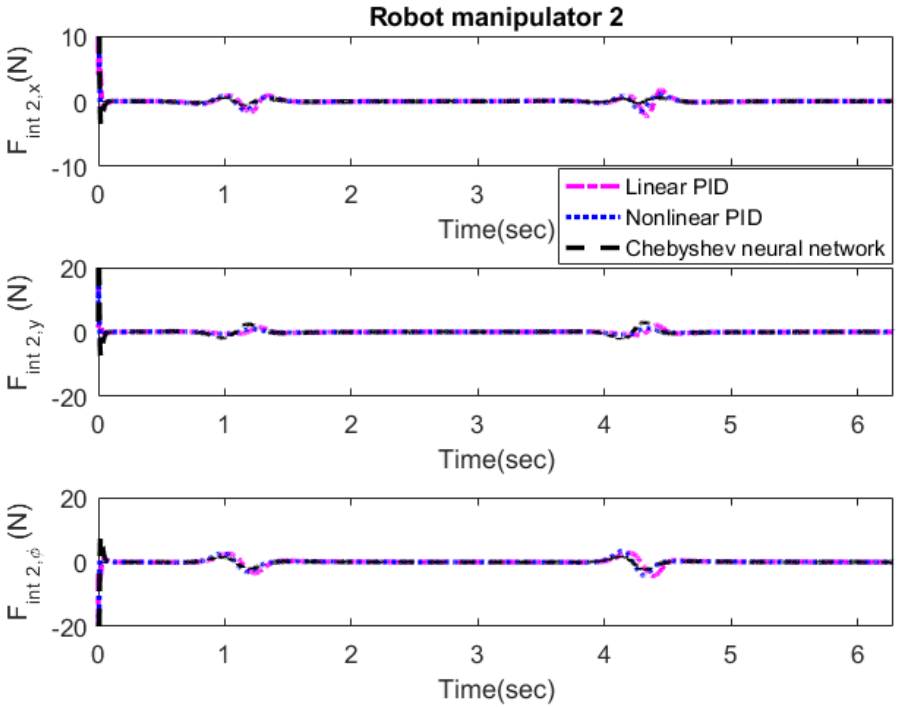

Fig. 11. Second robot's internal force tracking

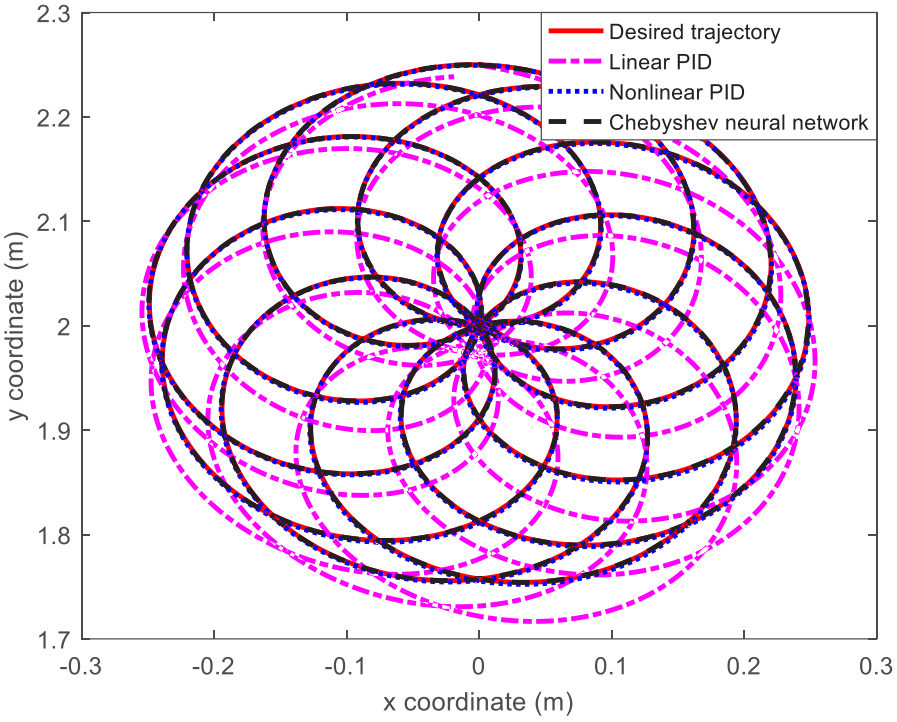

Fig. 12. Object trajectory tracking in the x-y plane

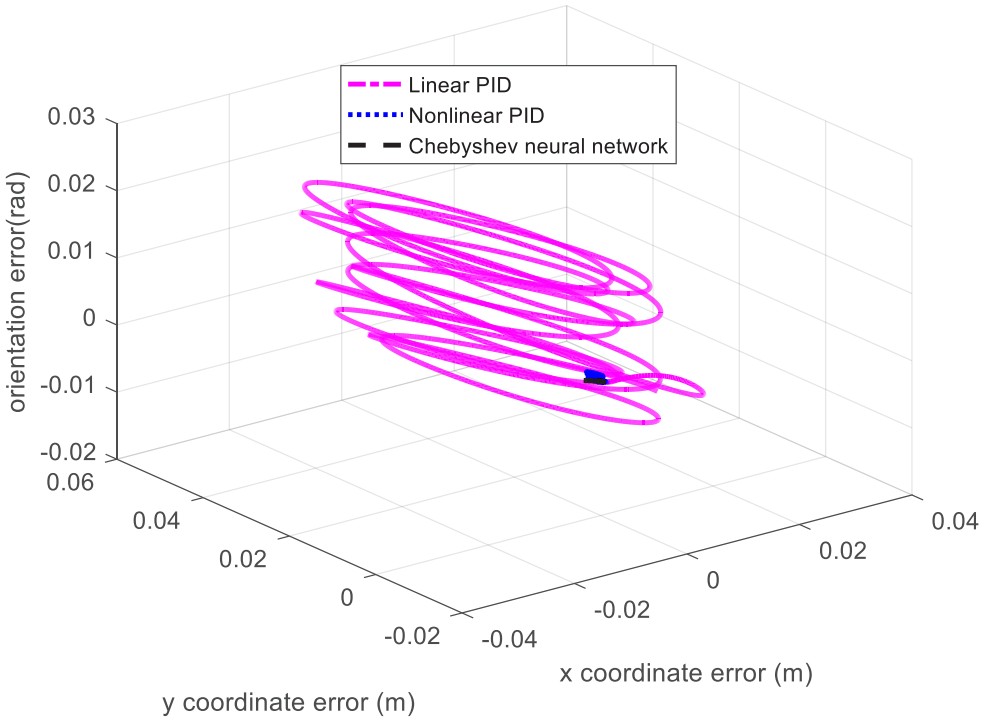

Fig. 13. Errors of orientation/position tracking

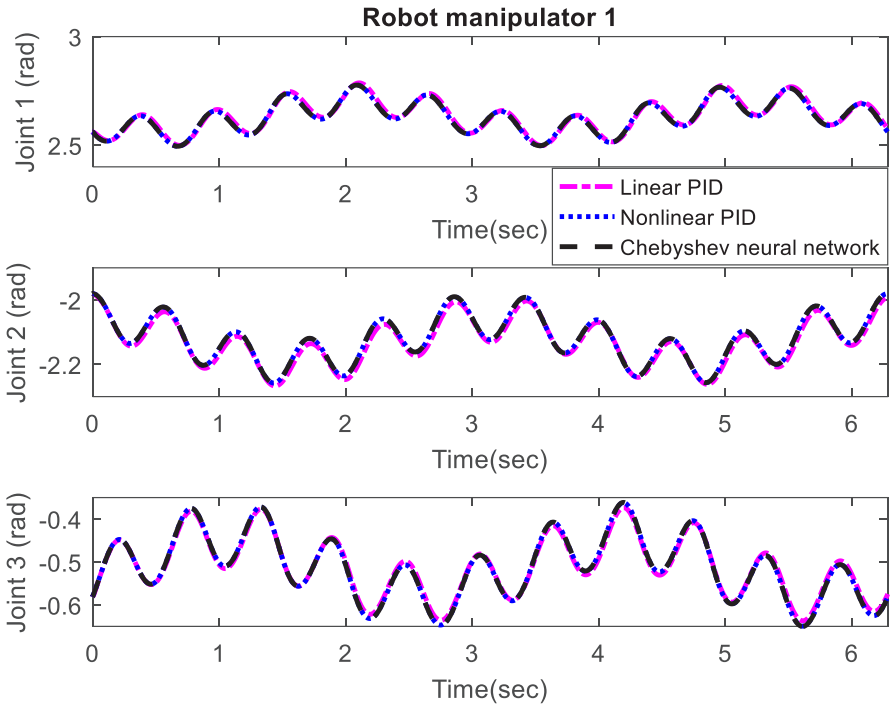

Fig. 14. First robot's joint angles while tracking the complicated trajectory

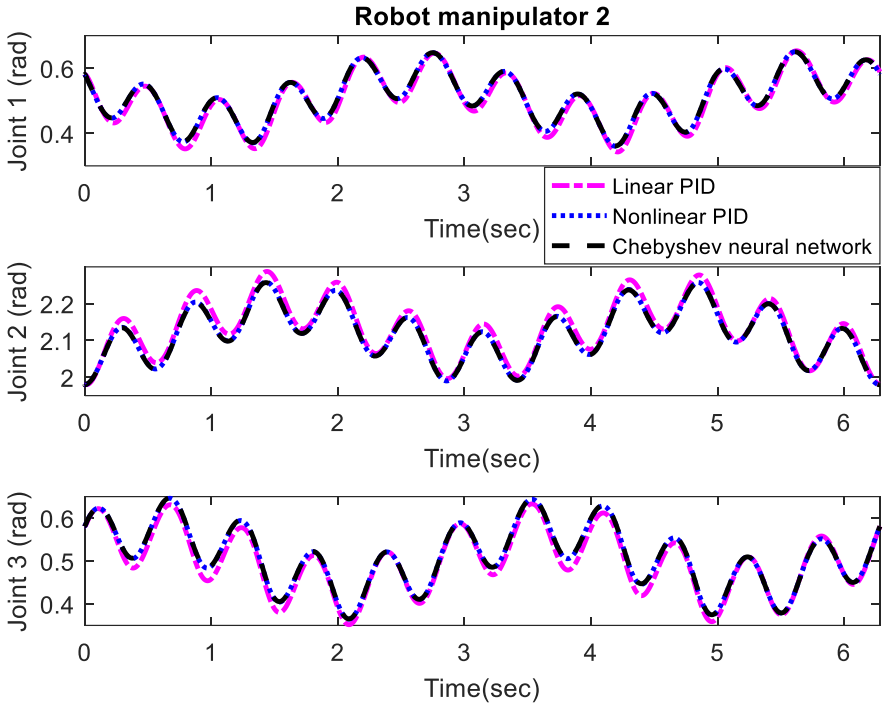

Fig. 15. Second robot's joint angles while tracking the complicated trajectory

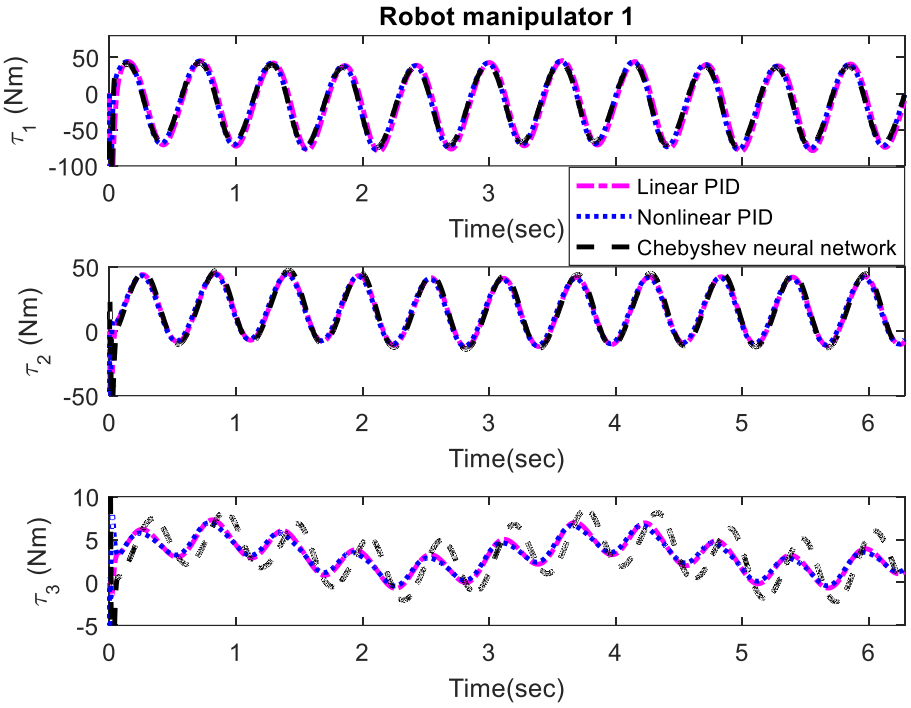

Fig. 16. First robot's control signals

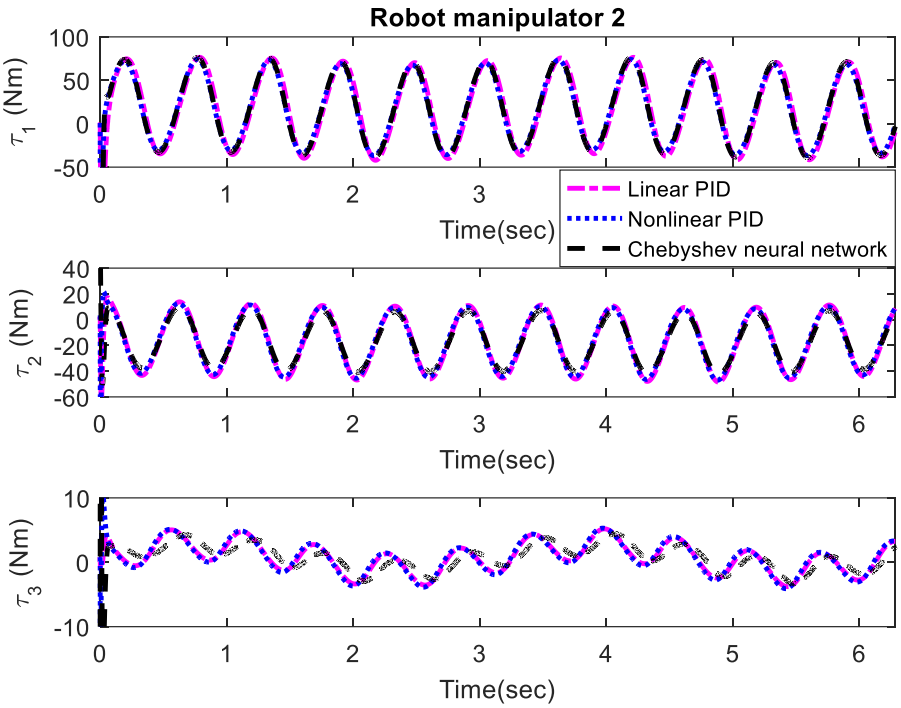

Fig. 17. Second robot's control signals

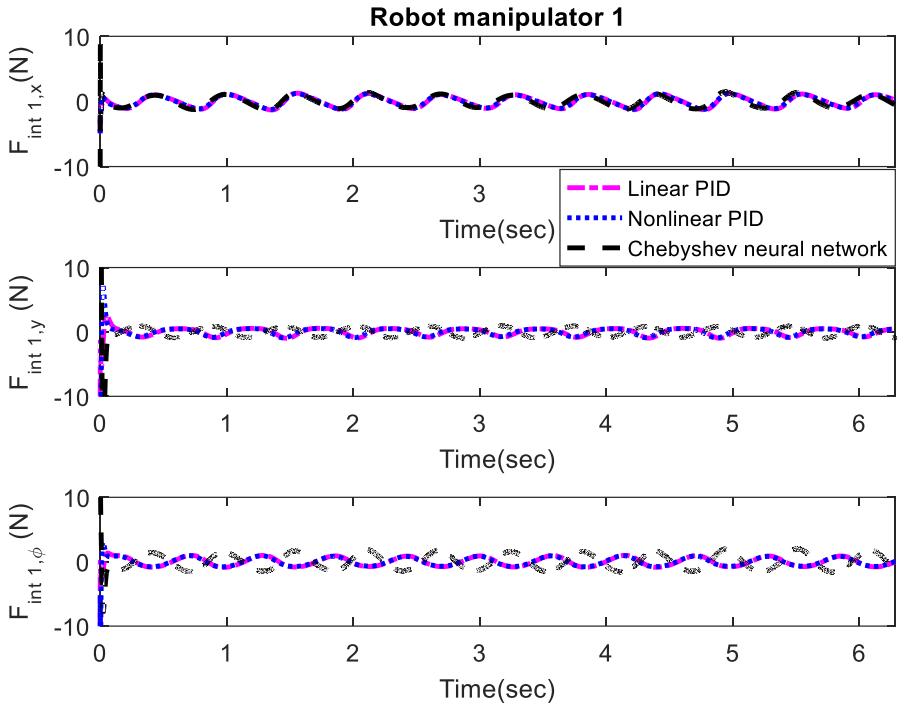

Fig. 18. First robot's internal force

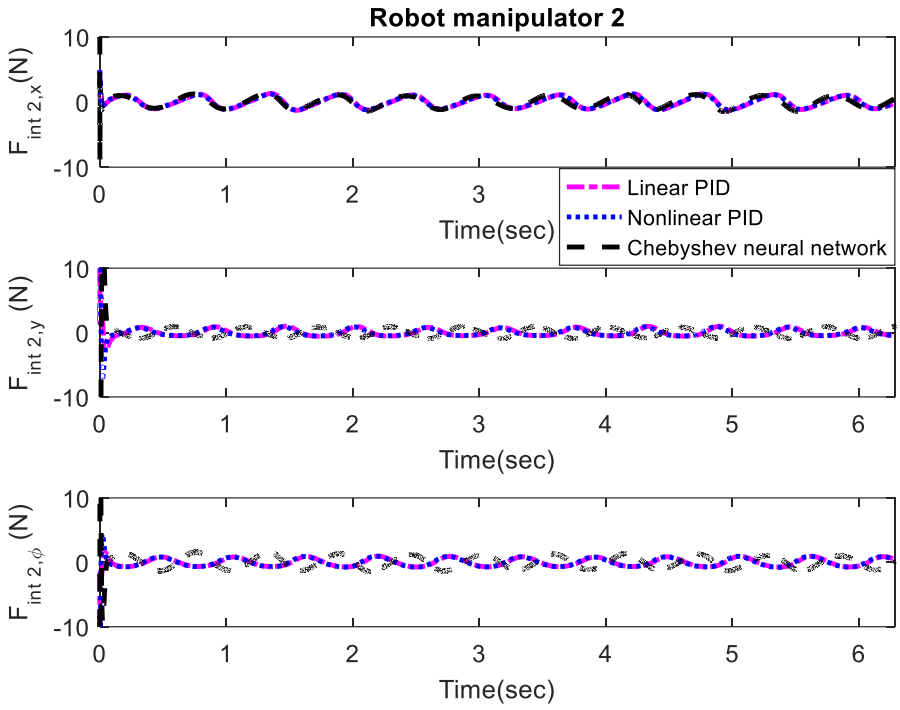

Fig. 19. The second robot's internal force

Table 2. Comparison of three performance indices

	Performance criterion		
Control approach	ISE	IAE	ITAE
The linear PID controller	0.006854	0.1952	0.5843
The nonlinear PID Controller	1.654×10^{-5}	0.009621	0.0187
The Chebyshev neural network-based approach	7.68×10^{-7}	0.001887	0.005779

based approach reduce all three indices, and the smallest values for these indexes are obtained by both schemes. However, in contrast to the Chebyshev neural network-based approach, there are very few tuning parameters in the nonlinear PID controller. The results have been summarized in Table 2.

6- Conclusion

This paper discusses the issue of managing the force-position of a load handled by numerous cooperative robots in the existence of unknown external perturbations and uncertainties. To address the problem, first, the system's dynamics, which include the robots and the carried load, were developed. Then, a linear and a nonlinear PID control structure was presented by allowing the payload to track the desired pose well. The internal force tracking problem is also taken into account by adding related terms to the control signal, such that stable load carrying is guaranteed. The UUB stability of all error signals is established by introducing an appropriate Lyapunov function. To examine the functioning of the proposed control scheme, it has been applied to two 3-DOF arms that carry an object cooperatively. Two

experiments involving simple and complex path tracking are considered, and both control structures are implemented in the system. The results indicate that despite the uncertainties and external perturbations, the nonlinear PID-controlled system has been able to track the desired internal force and position successfully. Therefore, the proposed nonlinear PID controller can be an effective choice for cooperative robotic systems. The results are also compared to those of a strong state-of-the-art approximator, the Chebyshev Neural Network.

Data Availability Statements

The data that support the findings of this study are available from the corresponding author upon reasonable request.

Compliance with Ethical Standards

The authors declare that this paper has never been submitted to other journals for simultaneous review processes and it has not been published before (partially or completely). Moreover, this paper has not been divided into different sections to have more submissions. The data has not been fabricated or changed in favor of the conclusions. In addition, no theory, data, or text belonging to other authors and publications was included as if it was our own, and proper acknowledgement of other works has been provided.

Disclosure of potential conflicts of interest

Funding: The authors did not receive any funding from any organization.

Conflict of Interest: No conflict of interest exists among the authors.

Research involving Human Participants and/or Animals

The authors declare that no human participant or animal was included in this work.

The authors state that this submission does not require any informed consent due to the fact that the results were acquired by computer simulation.

References

[1] Kallu, K. D. , Jie, W., and Lee, M. C., 2018, "Sensorless reaction force estimation of the end effector of a dual-arm robot manipulator using sliding mode control with a sliding perturbation observer". International Journal of Control, Automation and Systems, 16(3), pp. 1367-1378.

[2] Kim, H. H., Lee, M. C., Kyung, J. H., and Do, H. M., 2021, "Evaluation of Force Estimation Method Based on Sliding Perturbation Observer for Dual-arm Robot System". International Journal of Control, Automation and Systems, 19(1), pp. 1-10.

[3] Eid, J. J., and Oleynikov, D., 2021, "Cooperative and Miniature Robotics: Potential Applications in Surgery". In Digital Surgery, pp. 269-273, Springer, Cham. https://doi.org/10.1007/978-3-030-49100-0_20

[4] Poudel, L., Zhou, W., and Sha, Z. 2021, "Resource-Constrained Scheduling for Multi-Robot Cooperative 3D Printing". Journal of Mechanical Design, pp. 1-29. https://doi.org/10.1115/1.4050380

[5] Makris, S., 2021, Cooperative Manipulation-The Case of Dual Arm Robots". In Cooperating Robots for Flexible Manufacturing, Springer, Cham, pp. 123-132. https://doi.org/10.1007/978-3-030-51591-1_5

[6] Azizzadeh, H., Menhaj, M.B., and Talebi, H.A., 2019, "Model-based force/position control of cooperative manipulation systems". Automatica, 60 (1), pp. 113-123.

[7] Pizetta, I.H.B., Brandão, A.S., and Sarcinelli-Filho, M., 2019, "Avoiding obstacles in cooperative load transportation". ISA Transactions, 91, pp. 253-261.

[8] Chen, Y., and Lin, Y., 2020, "Combining model-based and model-free methods for stochastic control of distributed energy resources". Appl. Energy. 283: 116204 (2020)

[9] Hu, B., Guan, Z.H., Lewis, F.L., and Chen, C.P., 2020, "Adaptive tracking control of cooperative robot manipulators with markovian switched couplings". IEEE Transactions on Industrial Electronics, 68(3), pp. 2427-2436.

[10] Khan, A.T., Li, S., and Cao, X., 2021, "Control framework for cooperative robots in smart home using bio-inspired neural network". Measurement, 167, 108253.

[11] Wu, J., Jin, Z., Liu, A., and Yu, L., 2020, "Vision-based neural predictive tracking control for multi-manipulator systems with parametric uncertainty". ISA Transactions, 110, pp. 247-257

[12] Farahmandrad, M., Ganjefar, S., Talebi, H.A., and Bayati, M., 2019, "Fuzzy sliding mode controller design for a cooperative robotic system with uncertainty for handling an object". Journal of Dynamic Systems Measurements and Control, 141(6), pp. 1-8.

[13] Li, Y., Yang, C., Yan, W., Cui, R., and Annamalai, A., 2019, "Admittance-based adaptive cooperative control for multiple manipulators with output constraints". IEEE Transactions on Neural Networks Learning Systems, 30(12), pp. 3621-3632

[14] Hwang, C. L., Abebe, H. B., Chen, B. S., and Wu, F., 2020, "Fuzzy adaptive finite-time cooperative control with input saturation for nonlinear multiagent systems and its application". IEEE Access, 8, pp.105507-105520.

[15] Ngo, V. T., and Liu, Y. C., 2020, "Object transportation with force-sensorless control and event-triggered synchronization for networked uncertain manipulators". IEEE Transactions on Industrial Electronics, 68(1), pp. 902-912.

[16] Zhang, L., Sun, Y., Barth, A., and Ma, O., 2020, "Decentralized control of multi-robot system in cooperative object transportation using deep reinforcement learning". IEEE Access, 8, pp. 184109-184119.

[17] Izadbakhsh, A., Kalat, A. A. and Nikdel, N., 2022, "FAT-based robust adaptive controller design for electrically direct driven robots using Phillips q-Bernstein operators".

Robotica, 40(10), pp. 3415–3434

[18] Izadbakhsh, A., Zamani, I., and Khorashadizadeh, S., 2021, "Szász–Mirakyan-based adaptive controller design for chaotic synchronization". International Journal of Robust and Nonlinear Control, 31(5), pp.1689-1703, https://doi.org/10.1002/rnc.5380

[19] Nasiri, N., Fakharian A., and Menhaj M.B., 2020, "Observer-based robust control for flexible-joint robot manipulators: A state-dependent Riccati equation-based approach". Transactions of the institute of measurement and control, 42(16), pp. 3135-3155.

[20] Nasiri, N., Fakharian, A., and Menhaj, M.B., 2021, "A novel controller for nonlinear uncertain systems using a combination of SDRE and function approximation technique: Regulation and tracking of flexible-joint manipulators". Journal of the Franklin Institute, 358 (10), pp. 5185-5212.

[21] Nasiri, N., and Lademakhi, N. Y., 2021, "Nonlinear combined SMC-SDRE control versus SMC and SDRE approaches for electrical flexible-joint robots based on optimal observer". 9th RSI International Conference on Robotics and Mechatronics (ICRoM), pp. 568-573, doi: 10.1109/ICRoM54204.2021.9663514.

[22] Nasiri, N., Fakharian A., and Menhaj, M. B., 2022, "An Uncertain Optimal Factorization of Cooperative Manipulators for Robust Optimal Control Schemes". 30th International Conference on Electrical Engineering (ICEE), pp. 582-586, doi: 10.1109/ICEE55646.2022.9827024.

[23] Azar, A.T., Serrano, F.E., Hameed, I.A., and Kamal, N.A., 2020, "Vaidyanathan, S., Robust H-Infinity Decentralized Control for Industrial Cooperative Robots". In: Hassanien, A., Shaalan, K., Tolba, M. (eds) Proceedings of the International Conference on Advanced Intelligent Systems and Informatics 2019.. Advances in Intelligent Systems and Computing, 1058, Springer, Cham, https://doi.org/10.1007/978-3-030-31129-2_24

[24] Jose Guadalupe Romero, Emmanuel Nuño., and Carlos I. Aldana, 2021, "Robust PID consensus-based formation control of nonholonomic mobile robots affected by disturbances". International Journal of Control, DOI: 10.1080/00207179.2021.2015541.

[25] Ammar, H.H., and Azar, A.T., 2019," Robust Path Tracking of Mobile Robot Using Fractional Order PID Controller". In: Hassanien, A., Azar, A., Gaber, T., Bhatnagar, R., F. Tolba, M. (eds) The International Conference on Advanced Machine Learning Technologies and Applications (AMLTA2019). Advances in Intelligent Systems and Computing, 921. Springer, Cham. https://doi.org/10.1007/978-3-030-14118-9_37

[26] Deylami A., and Izadbakhsh A., 2022, "FAT-based robust adaptive control of cooperative multiple manipulators without velocity measurement". Robotica, 40 (6), pp.1732-1762, doi:10.1017/S0263574721001338.

[27] Izadbakhsh A, 2022, "An observer-based output tracking controller for electrically driven cooperative multiple manipulators with adaptive Bernstein-type approximator". Robotica, 40(7), pp. 2295-2319.

[28] Izadbakhsh, A., and Khorashadizadeh, S., 2021, "Polynomial-Based Robust Adaptive Impedance Control of Electrically Driven Robots". Robotica, 39(7), pp. 1181-1201.

[29] woon, L. C., Ge, S. S., Chen, X. Q., and Zhang, C., 1999, "Adaptive neural network control of coordinated manipulators". Journal of Robotic Systems, 16(4), pp.195-211.

[30] Qu. Z, and Dawson. D. M, 1996, "Robust tracking control of robot manipulators". IEEE Press, Inc., New York.

[31] Izadbakhsh, A., 2016, "Robust control design for rigid-link flexible-joint electrically driven robot subjected to constraint: theory and experimental verification". Nonlinear Dynamics, 85, pp. 751-765.

[32] Izadbakhsh, A., 2017, "A note on the "nonlinear control of electrical flexible-joint robots". Nonlinear Dynamics, 89, pp. 2753-2767.

[33] Tang H., and Li, Y., 2015, "Feedforward nonlinear PID control of a novel micromanipulator using Preisach hysteresis compensator". Robotics and Computer-Integrated Manufacturing, 34, pp. 124-132.

[34] Zhong, J., Fan, J., Zhu, Y., Zhao, J., and Zhai, W., 2014, "One nonlinear PID control to improve the control performance of a manipulator actuated by a pneumatic muscle actuator". Advances in Mechanical Engineering, 6, pp. 1727-1782.

[35] Diep Cong Thanh TU., and Ahn, K. K., 2006, "Nonlinear PID control to improve the control performance of 2 axes pneumatic artificial muscle manipulator using neural network". Mechatronics, 16, pp. 577–587.

[36] Lee, J., Chang, P. H. , Yu B., and Jin, M., 2020, "An Adaptive PID Control for Robot Manipulators Under Substantial Payload Variations". IEEE Access, 8, pp. 162261-162270.

[37] Maddi, A., Guessoum, A., and Berkani D., 2014, "Design of Nonlinear PID Controllers Based on Hyper-Stability Criteria". 15th international conference on science and techniques of automatic control and computer engineering, pp. 736-741.

[38] Ghediri, A.,Lamamra, K., Ait Kaki, A., and Vaidyanathan, S., 2022, "Adaptive PID computed-torque control of robot manipulators based on DDPG reinforcement learning". International Journal of Modelling, Identification and Control, 41(3), pp.173-182

[39] Perrusquia, A., Yu, W., and Soria, A., 2019, "Position/Force control of Robot Manipulators Using Reinforcement Learning". Industrial Robot, 46 (2), pp. 267-280.

[40] Korayem, M. H., and Nekoo, S. R., 2018, "Controller design of Cooperative Manipulators using state-

dependent Ricatti equation". Robotica, 36(4), pp. 484-515.

[41] Kelly, R., Santibanez, V., and Loria, A., 2005, "Control of Robot Manipulators in Joint Space". Springer-Verlag London Limited.

[42] Izadbakhsh, A., Nikdel, N., and Deylami, A., 2021, "Cooperative and robust object handling by multiple manipulators based on the differential equation approximator". ISA Transaction, 128, Part B, pp. 68-80.

[43] Izadbakhsh, A., and Nikdel, N., 2022, "Robust adaptive control of cooperative multiple manipulators based on the Stancu-Chlodowsky universal approximator". Communications in Nonlinear Science and Numerical Simulation, 111, 106471, https://doi.org/10.1016/j.cnsns.2022.106471

[44] Patra, J. C., and Kot, A. C., 2002, "Nonlinear dynamic system identification using chebyshev functional link artificial neural networks". IEEE Transactions On Systems, man and Cybernetics, Part B, 32, pp. 505-511.

[45] Purwar, S., Kar, I. N., and Jha, A. N., 2008, "Adaptive output feedback tracking control of robot manipulators using position measurements only". Expert systems with Applications, 34,pp. 2789-2798.

Appendix I:

Proof is similar to that reference [30] and based on Gershgorin theorem, when $\alpha_1 = \alpha_2 = \mu$. Let $\mathbf{T}$ be a transformation such that

$$\mathbf{M}_c = \mathbf{T}^{-1}\mathbf{\Lambda}\mathbf{T} \tag{A1}$$

where $\mathbf{\Lambda} = diag(a_1, a_2, ..., a_n)$ and the a_i 's are the point-wise eigenvalues of $\mathbf{M}_c$. It follows that:

$$\begin{bmatrix} \mathbf{T}^{-1} & \mathbf{0}_n & \mathbf{0}_n \\ \mathbf{0}_n & \mathbf{T}^{-1} & \mathbf{0}_n \\ \mathbf{0}_n & \mathbf{0}_n & \mathbf{T}^{-1} \end{bmatrix} \boldsymbol{P} \begin{bmatrix} \mathbf{T} & \mathbf{0}_n & \mathbf{0}_n \\ \mathbf{0}_n & \mathbf{T} & \mathbf{0}_n \\ \mathbf{0}_n & \mathbf{0}_n & \mathbf{T} \end{bmatrix} = \frac{1}{2}\begin{bmatrix} \mu\boldsymbol{\kappa}_p + \mu\boldsymbol{\kappa}_I + \mu^2\mathbf{\Lambda} & \mu\boldsymbol{\kappa}_d + \boldsymbol{\kappa}_I + \mu^2\mathbf{\Lambda} & \mu\mathbf{\Lambda} \\ \mu\boldsymbol{\kappa}_d + \boldsymbol{\kappa}_I + \mu^2\mathbf{\Lambda} & \mu\boldsymbol{\kappa}_d + \boldsymbol{\kappa}_p + \mu^2\mathbf{\Lambda} & \mu\mathbf{\Lambda} \\ \mu\mathbf{\Lambda} & \mu\mathbf{\Lambda} & \mathbf{\Lambda} \end{bmatrix} \in \Re^{3n\times 3n} \tag{A2}$$

By the Gershgorin theorem, it can be easily shown that the eaigenvalues $\aleph_j$ for j=1,…,*n*, of the matrix (A2) satisfy the following inequalities

$$\begin{aligned} &\left|\aleph_i - \frac{1}{2}(\mu\kappa_{Ii} + \mu\kappa_{pi} + \mu^2 a_i)\right| \le \frac{1}{2}(\mu\kappa_{di} + \kappa_{Ii} + (1+\mu)\mu a_i) \\ &\left|\aleph_{n+i} - \frac{1}{2}(\mu\kappa_{di} + \kappa_{pi} + \mu^2 a_i)\right| \le \frac{1}{2}(\mu\kappa_{di} + \kappa_{Ii} + (1+\mu)\mu a_i) \\ &\left|\aleph_{2n+i} - \frac{1}{2}a_i\right| \le \mu a_i \end{aligned} \tag{A3}$$

Or equivalently

$$\begin{aligned}
&\mu(\kappa_{pi}-\kappa_{di})+(\mu-1)\kappa_{Ii}-\mu a_i \le 2\aleph_i \le (1+\mu)\kappa_{Ii}+\mu(\kappa_{pi}+\kappa_{di})+(1+2\mu)\mu a_i \\
&\kappa_{pi}-\mu a_i-\kappa_{Ii} \le 2\aleph_{n+i} \le \kappa_{pi}+2\mu\kappa_{di}+\kappa_{Ii}+\mu a_i(2\mu+1) \\
&a_i(1-2\mu) \le 2\aleph_{2n+i} \le a_i(1+2\mu)
\end{aligned} \tag{A4}$$

Now, considering the inequalities $\xi_m \le a_i \le \xi_M$, $\lambda_{\min}(\boldsymbol{\kappa}_p) \le \kappa_{pi} \le \lambda_{\max}(\boldsymbol{\kappa}_p)$, $\lambda_{\min}(\boldsymbol{\kappa}_I) \le \kappa_{Ii} \le \lambda_{\max}(\boldsymbol{\kappa}_I)$, and $\lambda_{\min}(\boldsymbol{\kappa}_d) \le \kappa_{di} \le \lambda_{\max}(\boldsymbol{\kappa}_d)$ for i=1,2,..,n and the proof is completed.■

Appendix II:

1- Derivation of (50)

Using the definitions of $\mathbf{M}_c(\mathbf{x}_o)$, and $\mathbf{G}_c(\mathbf{x}_o)$, it is straightforward to present that

$$\left\|\mathbf{M}_c(\mathbf{x}_o)\right\| \le \frac{\sigma^2_{\max}(\mathbf{J}_o(\mathbf{x}_o))}{\xi^2_{J_e,\min}}\xi_D + \xi_{D_o} = \xi_M \tag{B1}$$

$$\left\|\mathbf{G}_c(\mathbf{x}_o)\right\| \le \xi_{G_o} + \frac{\sigma_{\max}(\mathbf{J}_o(\mathbf{x}_o))}{\xi_{J_e,\min}}(\xi_G+\xi_\tau) \tag{B2}$$

where we have utilized inequalities (4), (6), (7), (8), (15), (17), and (18). Furthermore, using inequalities (4), (5), (7), (16), (18), (55), definition of $\mathbf{C}_c(\mathbf{x}_o,\dot{\mathbf{x}}_o)$, and based on the same manipulation as before, it is clear that

$$\left\|\mathbf{C}_c(\mathbf{x}_o,\dot{\mathbf{x}}_o)\right\| \le L_0\left\|\dot{\mathbf{x}}_o\right\| \tag{B3}$$

where

$$L_0 = \frac{\sigma_{\max}(\mathbf{J}_o(\mathbf{x}_o))}{\xi_{J_e,\min}}\xi_D\left(\frac{\sigma^2_{\max}(\mathbf{J}_o(\mathbf{x}_o))\xi_{dJ_e}}{\xi^3_{J_e,\min}}+\frac{\xi_{dJ_o}}{\xi_{J_e,\min}}\right)+\left(\frac{\sigma^3_{\max}(\mathbf{J}_o(\mathbf{x}_o))}{\xi^3_{J_e,\min}}\xi_C+\xi_{C_o}\right)$$

and (7), (18), and (55) have been utilized. Then, inequality (B4) can be easily obtain by considering (B1), (B2), (B3), (27), (33), and some mathematical calculation

$$\begin{aligned}
\left\|\boldsymbol{\Delta}(t)\right\| &\le \left\|\mathbf{M}_c(\mathbf{x}_o)\right\|A_M + \left\|\mathbf{G}_c(\mathbf{x}_o)\right\| + \left\|\mathbf{C}_c(\mathbf{x}_o,\dot{\mathbf{x}}_o)\right\|\left\|\dot{\mathbf{x}}_o\right\| \\
&\le \xi_M A_M + \frac{\sigma_{\max}(\mathbf{J}_o(\mathbf{x}_o))}{\xi_{J_e,\min}}(\xi_G+\xi_\tau)+\xi_{G_o}+L_0\left\|\dot{\mathbf{x}}_o\right\|^2
\end{aligned} \tag{B4}$$

Using the definitions of (54), and some simplification, inequality (53) is derived in which

$$\beta_0 = \xi_M A_M + \frac{\sigma_{\max}(\mathbf{J}_o(\mathbf{x}_o))}{\xi_{J_e,\min}}(\xi_G+\xi_\tau)+\xi_{G_o}+L_0 V_M^2 \tag{B5}$$

HOW TO CITE THIS ARTICLE
A. Izadbakhsh, N. Nasiri, M. B. Menhaj, Linear/Nonlinear PID Control of Cooperative Multiple Robot Manipulators: A Robust Approach, AUT J. Model. Simul., 55(1) (2023) 71-98.

DOI: 10.22060/miscj.2023.21867.5305